Modeling and Simulation of Conditionally Volume Averaged Viscoelastic Two-Phase Flows

Florian Habla
Catalysis Research Center and Chemistry Department, Technische Universität München, Lichtenbergstraße 4, D-85748 Garching b. München, Germany

Laura Dietsche
The Dow Chemical Company, Midland, MI 48674

Kai-Olaf Hinrichsen
Catalysis Research Center and Chemistry Department, Technische Universität München, Lichtenbergstraße 4, D-85748 Garching b. München, Germany

DOI 10.1002/aic.14095
Published online April 2, 2013 in Wiley Online Library (wileyonlinelibrary.com)

Conditional volume averaging is used to develop a model capable of simulating two-phase flows of viscoelastic fluids with surface tension effects. The study is started with the single-phase mass and momentum balances, which are subsequently conditionally volume averaged. In doing so, we arrive at a set of equations having unclosed interfacial terms, for which closure relations for viscoelastic fluids are presented. The resulting equations possess a structure similar to the single-phase equations; however, separate conservation equations are solved for each phase. As a result, each phase has its own pressure and velocity over the entire domain. Next, our numerical implementation is briefly outlined. We find that a Poiseuille single-phase flow is predicted correctly. The closure terms are examined by considering a two-phase shearing flow and a quiescient cylinder with surface tension. A convergence analysis is performed for a steady stratified two-phase flow with both phases being viscoelastic. © 2013 American Institute of Chemical Engineers *AIChE J*, 59: 3914–3927, 2013

Keywords: two-phase flow, viscoelasticity, rheology, volume averaging, Oldroyd-B

Introduction

Viscoelastic two-phase flows can be found in a broad range of industrial applications such as injection molding,[1] polymer blending,[2] and coextrusion.[3] Understanding and predicting the fluid's behavior is a major research challenge. The key issue is dealing with both complex fluid behavior, including viscous and elastic effects, as well as multiphase flows. These types of flows comprise a variety of spatial and temporal scales. The spatial scales are ranging from microscale of the molecular conformation to the mesoscale of the interfacial morphology, and up to the macroscale of the hydrodynamics of the flow. On the other hand, the temporal scales range from the time-scale of molecular conformation changes up to the duration of the experiment. These aspects complicate the requirements of the numerical treatment.

Over the years, many techniques have evolved to address the multiphase treatment, which can be subdivided into sharp interface and diffuse interface methods.

A conceptual straightforward approach for sharp interface methods is to use a moving mesh with the nodes deforming according to the boundary motion. This approach is used, for example, in Cristini et al.[4] However, the necessity of remeshing leads to huge amounts of additional computational costs and interpolation errors. Moreover, changes in the interfacial topology when facing breakup or coalescence are intractable using such a methodology.

In contrast, in diffuse interface methods, the interface possesses a finite width with the physical properties, such as density and viscosity, smoothly varying across the interface.[5] The Volume-of-Fluid (VoF) originally proposed by Hirt and Nichols[6] is one of these methods. The volume fraction is used as an order parameter to determine, which phase is present in a particular volume. This order parameter is convected as an invariant of the flow field. However, one of the major disadvantages of the VoF method is the difficulty to accurately reconstruct the interfacial morphology such as curvature and interface normal vector from the order parameter. Kim et al.[7] applied a VoF method to viscoelastic free-surface flows to simulate three-dimensional jet buckling. More recently, Habla et al.[8] applied a finite-volume-based VoF method to a variety of complex multiphase problems, including die extrusion, rod-

Correspondence concerning this article should be addressed to K-O. Hinrichsen at olaf.hinrichsen@ch.tum.de.

climbing, and droplet deformations in shear and elongational flows. The level-set method was also successfully applied to two-phase flows[9,10] and more recently to viscoelastic two-phase flows.[11] In the level-set method, the interface is defined as the zero level set of a smooth auxiliary function. Interfacial forces such as surface tension are smoothed across the interface.[9] Although the interface remains sharp in this treatment, the conservation of mass cannot be guaranteed. Some authors developed a hybrid approach making use of the advantages of both the VoF and the level-set methods.[12,13] This approach is called coupled level-set volume-of-fluid method and was more recently applied to simulating bubble and drop motion of a Finitely Extensible Non-Linear Elastic – Chilcott Rallison (FENE-CR) fluid.[14] Another diffuse-interface approach was developed by Unverdi and Tryggvason[15,16] called front-tracking. In front-tracking, an interface indicator function is artificially spread over a few computational cells from the known sharp interface position. Subsequently, this indicator function is used to convect the interface. Being thermodynamically derived, the phase-field method is another type of diffuse-interface methods, which was recently adapted by Yue et al.[17,18] to simulate deformation and head-on collision of droplets with either phase being an Oldroyd-B type fluid.

A common aspect of the aforementioned diffuse-interface methods is that they consist of only one set of conservation equations, that is, mass and momentum, wherein the fluid properties vary across the interface smoothly using a phase indicator function. Advantages of diffuse interface methods are, that a fixed grid can be used in an Eulerian treatment, and that large distortions of the interface, occurring, for example, in breakup and coalescence, are handled in a straightforward manner and will not affect the numerical simulation. However, due to the numerical necessity of artificially smearing the interface, problems may arise if the width of the smeared interface is on the order of the considered phenomena, which is the case, for example, in breakup and coalescence of droplets. Furthermore, due to the artificial smearing of the interface, the results obtained strongly depend upon the way the indicator function varies across the interface. This is particularly distinct if the fluids possess large property differences. As a result, a model, in which the results are independent of the interface width, such that the interface width can be chosen arbitrarily large, is highly needed.

The technique of averaging is commonly used for deriving two-phase models for large-scale two-phase flows such as bubbly and particulate flows. The averaging is done on a larger scale compared to the dispersed phase elements. Consequently, the interfacial scale is not resolved and coupling between the phases is accounted for only in an average sense. However, Beckermann recently applied ensemble averaging on an atomic scale to the local single-phase equations to arrive at a model suitable for direct simulation of two-phase flows.[19–21] Herein, the averaging is applied on a much smaller scale compared to the interfacial averaging methods, so as to partly resolve the interfacial morphology and the flows inside the interface. In contrast to commonly used diffuse-interface methods, wherein only a single velocity and pressure is present even in the interfacial region, the ensemble averaged two-phase model by Beckermann and coworkers treats both phases separately with each phase having its own velocity and pressure. As a consequence, separate conservation equations for mass and momentum have to be solved, which is common for the interfacial averaged two-phase models. These equations are explicitly coupled using closure relations to account for the phase interaction. Beckermann showed that the resulting model possesses the important property of being independent of the chosen interface width; however, this is only the case with zero surface tension.[20]

In this work, we will apply the technique of conditional volume averaging to the mass and momentum equations, but on a larger scale compared to Sun and Beckermann.[20] Our model is motivated by the desire to predict mesoscale and macroscale flows by underresolving microscale structures, rather than a need to resolve the scale of the fluctuating atomic structures inside the diffuse interface to allow direct numerical simulation. That is, the mean interfacial curvature is resolved and large compared to the interfacial width. The resulting model will be based on local instantaneous conservation equations, which are transformed using the mathematically well-grounded conditional volume averaging technique. The resulting coupling terms are then physically interpreted by splitting them into resolved and unresolved portions. A drawback of treating both phases separately is that they require a model for the coupling terms, which is usually based on simple concepts.[20] In this work, we will present closure relations to couple our derived set of equations based on the above-mentioned ideas. In doing so, the stress terms are treated using the well-known Oldroyd-B constitutive equation, see, for example, Bird et al.,[22] to allow for either phase being viscoelastic. By solving each phase separately, no *a priori* defined variation of variables across the interface has to be postulated. Moreover, both phases coexist inside the interfacial region thus avoiding rapid changes in the properties across the interface.

Mathematical Formulation

Conditional averaging

First, we will shortly outline the concept of conditional volume averaging. For further reading, we would like to refer the reader to the literature.[23–27]

To distinguish between multiple phases, the phase indicator function $I_\varphi(\mathbf{x},t)$ is introduced, which equals one, if phase φ is present and is zero elsewhere

$$I_\varphi(\mathbf{x},t)=\begin{cases}1 & \text{if point } (\mathbf{x},t) \text{ is in phase } \varphi\\ 0 & \text{otherwise}.\end{cases} \tag{1}$$

As a result of Eq. 1, the following must hold for N phases

$$\sum_{i=1}^{N} I_i(\mathbf{x},t)=1 \tag{2}$$

Let $\mathbf{Q}$ be any local instantaneous physical property, for example, a scalar, vector, or tensor. Multiplication of the phase indicator function $I_\varphi(\mathbf{x},t)$ with $\mathbf{Q}$ gives $\mathbf{Q}_\varphi \equiv I_\varphi(\mathbf{x},t)\mathbf{Q}$, where $\mathbf{Q}_\varphi$ denotes the conditioned quantity.

Volume averaging of a local instantaneous physical property $\mathbf{Q}$ using an arbitrary averaging volume element $\delta\mathrm{V}$ is defined as

$$\overline{\mathbf{Q}}^{\partial\mathrm{V}} \equiv \frac{1}{\delta\mathrm{V}}\int_{\delta V}\mathbf{Q}(\mathbf{x},t)d\mathbf{y} \tag{3}$$

where $\delta\mathrm{V}$ is the averaging volume and the vector $\mathbf{y}$ is a relative position vector pointing inside the volume $\delta\mathrm{V}$. In the remainder, the index $\delta\mathrm{V}$ will be dropped due to brevity.

Now consider the volume average of the phase indicator function $I_\varphi(\mathbf{x},t)$

$$\alpha_\varphi(\mathbf{x},t) = \overline{I_\varphi(\mathbf{x},t)} \tag{4}$$

then $\alpha_\varphi(\mathbf{x},t)$ is the phase volume fraction, which in the case of ensemble averaging can be thought of the probability of a point $(\mathbf{x},t)$ pertaining to phase φ. Note that $(\mathbf{x},t)$ will be dropped for $I_\varphi(\mathbf{x},t)$ and $\alpha_\varphi(\mathbf{x},t)$ and will solely be denoted as I_φ and α_φ in the remainder.

The conditional volume average of a local instantaneous physical property $\mathbf{Q}$ is then defined as follows[23]

$$\overline{I_\varphi \mathbf{Q}} = \alpha_\varphi \overline{\mathbf{Q}}_\varphi \tag{5}$$

The conditional fluctuation is the difference between the local instantaneous and conditional volume average of the property[27]

$$\mathbf{Q}'_\varphi = \mathbf{Q} - \overline{\mathbf{Q}}_\varphi \tag{6}$$

The conditional volume averaged product of $\mathbf{Q}$ and another property $\mathbf{P}$ is

$$\overline{I_\varphi \mathbf{P}\mathbf{Q}} = \alpha_\varphi \overline{\mathbf{P}}_\varphi \overline{\mathbf{Q}}_\varphi + \alpha_\varphi \overline{\mathbf{P}'_\varphi \mathbf{Q}'_\varphi} \tag{7}$$

In order to apply conditional volume averaging to the mass and momentum equations, we additionally need to consider conditional volume averaged differential operations. It is worth noting here that differential operators and the averaging operation commute

$$\overline{\nabla\left(I_\varphi \mathbf{Q}\right)} = \nabla\overline{\left(I_\varphi \mathbf{Q}\right)} = \nabla\left(\alpha_\varphi \overline{\mathbf{Q}}_\varphi\right) \tag{8}$$

and

$$\overline{\frac{\partial I_\varphi \mathbf{Q}}{\partial t}} = \frac{\partial \overline{I_\varphi \mathbf{Q}}}{\partial t} = \frac{\partial\left(\alpha_\varphi \overline{\mathbf{Q}}_\varphi\right)}{\partial t} \tag{9}$$

Now consider the conditional volume average of $I_\varphi \nabla \mathbf{Q} = \nabla\left(I_\varphi \mathbf{Q}\right) - \left(\nabla I_\varphi\right)\mathbf{Q}$ over a control volume $\partial \mathrm{V}$. ∇I_φ is nonzero only at the interface, where it has a value of infinity thus resembling the Dirac delta function and the direction $\mathbf{n}_{I,\varphi}$ normal to the interface pointing inside of the volume φ. Then, the conditional volume average of $I_\varphi \nabla \mathbf{Q}$ is

$$\begin{aligned}\overline{I_\varphi \nabla \mathbf{Q}} &= \overline{\nabla\left(I_\varphi \mathbf{Q}\right)} - \overline{\left(\nabla I_\varphi\right)\mathbf{Q}} \\ &= \nabla\left(\alpha_\varphi \overline{\mathbf{Q}}_\varphi\right) - \lim_{\delta \mathrm{V}\to 0} \overline{\frac{1}{\delta \mathrm{V}} \int_{S(\mathbf{x},t)} \mathbf{n}_{I,\varphi} \mathbf{Q} dS} \\ &= \nabla\left(\alpha_\varphi \overline{\mathbf{Q}}_\varphi\right) - \widehat{\mathbf{n}_{I,\varphi} \mathbf{Q}} \Sigma\end{aligned}$$

where $S(\mathbf{x},t) = 0$ is the equation of the interface, Σ is the interfacial area density

$$\Sigma \equiv \lim_{\delta \mathrm{V}\to 0} \overline{\frac{1}{\delta \mathrm{V}} \int_{S(\mathbf{x},t)} dS} \tag{11}$$

and $\widehat{\mathbf{Q}}$ denotes the interface average of a property $\mathbf{Q}$[27]

$$\widehat{\mathbf{Q}} \equiv \frac{\lim_{\delta \mathrm{V}\to 0} \overline{\frac{1}{\delta \mathrm{V}} \int_{S(\mathbf{x},t)} \mathbf{Q} dS}}{\Sigma} \tag{12}$$

The conditionally volume averaged divergence of the property $\mathbf{Q}$ can be obtained analogously

$$\begin{aligned}\overline{I_\varphi \nabla \cdot \mathbf{Q}} &= \overline{\nabla \cdot \left(I_\varphi \mathbf{Q}\right)} - \overline{\left(\nabla I_\varphi\right) \cdot \mathbf{Q}} \\ &= \nabla \cdot \left(\alpha_\varphi \overline{\mathbf{Q}}_\varphi\right) - \lim_{\delta \mathrm{V}\to 0} \overline{\frac{1}{\delta \mathrm{V}} \int_{S(\mathbf{x},t)} \mathbf{n}_{I,\varphi} \cdot \mathbf{Q} dS} \\ &= \nabla \cdot \left(\alpha_\varphi \overline{\mathbf{Q}}_\varphi\right) - \widehat{\mathbf{n}_{I,\varphi} \cdot \mathbf{Q}} \Sigma\end{aligned} \tag{13}$$

For the time derivative, we obtain

$$\begin{aligned}\overline{I_\varphi \frac{\partial \mathbf{Q}}{\partial t}} &= \overline{\frac{\partial I_\varphi \mathbf{Q}}{\partial t}} - \overline{\mathbf{Q} \frac{\partial I_\varphi}{\partial t}} = \frac{\partial\left(\alpha_\varphi \overline{\mathbf{Q}}_\varphi\right)}{\partial t} + \overline{\mathbf{Q}\left(\left(\nabla I_\varphi\right) \cdot \mathbf{U}_I\right)} \\ &= \frac{\partial\left(\alpha_\varphi \overline{\mathbf{Q}}_\varphi\right)}{\partial t} + \lim_{\delta \mathrm{V}\to 0} \overline{\frac{1}{\delta \mathrm{V}} \int_{S(\mathbf{x},t)} \mathbf{Q}\left(\mathbf{n}_{I,\varphi} \cdot \mathbf{U}_I\right) dS} \\ &= \frac{\partial\left(\alpha_\varphi \overline{\mathbf{Q}}_\varphi\right)}{\partial t} + \widehat{\mathbf{Q}\left(\mathbf{n}_{I,\varphi} \cdot \mathbf{U}_I\right)} \Sigma\end{aligned}$$

which follows from the fact that the phase indicator function I_φ is convected with the velocity of the interface $\mathbf{U}_I$

$$\frac{\partial I_\varphi}{\partial t} + \left(\nabla I_\varphi\right) \cdot \mathbf{U}_I = 0 \tag{15}$$

A useful identity can be obtained from Eq. 10 with $\mathbf{Q} = 1$

$$\nabla \alpha_\varphi = \widehat{\mathbf{n}_{I,\varphi}} \Sigma \tag{16}$$

Moreover, by using Eq. 14 with $\mathbf{Q} = 1$, one can derive the evolution equation for the volume fraction α_φ of phase φ

$$\frac{\partial \alpha_\varphi}{\partial t} + \widehat{\mathbf{n}_{I,\varphi} \cdot \mathbf{U}_I} \Sigma = 0 \tag{17}$$

Similar to decomposing the local instantaneous quantity into a volume average and a fluctuation (Eq. 6), an interfacial quantity $\mathbf{Q}_I$ (a quantity defined solely on the interface) may also be decomposed into a surface average and surface fluctuation

$$\mathbf{Q}_I = \widehat{\mathbf{Q}} + \mathbf{Q}^{\#} \tag{18}$$

Although the general approach is valid for any number of phases (see Eq. 2), we restrict the derivation in the subsequent section to the case of two phases (φ and ω).

Conservation equations

In this section, we will apply conditional volume averaging to derive a set of equations from the local instantaneous mass and momentum conservation suitable for describing multiphase flows, in which we seek to capture the interfacial morphologies on a mesoscale, while underresolving the microscale structures. The derivation of the conditional volume averaged continuity and momentum equations in particular follows the derivation of Ref. 27. However, in Ref. 27 a model for simulating interfacial averaged bubbly multiphase flows is derived, with one phase being dispersed in another phase. Throughout this work, we will consider transient, isothermal two-phase flows of incompressible viscoelastic fluids.

Conditionally volume averaged mass conservation

The local instantaneous continuity equation is

$$\frac{\partial \rho}{\partial t} + \nabla \cdot (\rho \mathbf{U}) = 0 \tag{19}$$

where ρ is the density and $\mathbf{U}$ is the velocity.

Conditional volume averaging of the local instantaneous continuity equation for phase φ gives

$$\overline{I_\varphi \frac{\partial \rho}{\partial t}} + \overline{I_\varphi \nabla \cdot (\rho \mathbf{U})} = 0 \tag{20}$$

Using Eqs. 13 and 14 gives

$$\frac{\partial (\alpha_\varphi \overline{\rho}_\varphi)}{\partial t} + \widehat{\rho (\mathbf{n}_{I,\varphi} \cdot \mathbf{U}_I)} \Sigma + \nabla \cdot (\alpha_\varphi \overline{\rho}_\varphi \overline{\mathbf{U}}_\varphi) - \widehat{\rho (\mathbf{n}_{I,\varphi} \cdot \mathbf{U})} \Sigma = 0 \tag{21}$$

Note here that due to the assumption of incompressible fluids no density weighted averages appear. The interface contribution terms can be grouped together

$$\frac{\partial (\alpha_\varphi \overline{\rho}_\varphi)}{\partial t} + \nabla \cdot (\alpha_\varphi \overline{\rho}_\varphi \overline{\mathbf{U}}_\varphi) = \widehat{\rho (\mathbf{n}_{I,\varphi} \cdot (\mathbf{U} - \mathbf{U}_I))} \Sigma \tag{22}$$

Assuming no mass transfer, that is, $\mathbf{U} - \mathbf{U}_I = 0$, and by dividing Eq. 22 by the constant density $\overline{\rho}_\varphi$, one obtains

$$\frac{\partial \alpha_\varphi}{\partial t} + \nabla \cdot (\alpha_\varphi \overline{\mathbf{U}}_\varphi) = 0 \tag{23}$$

Note that the same equation holds for the second phase ω by simply changing the indices.

Conditionally volume averaged momentum conservation

The local instantaneous momentum equation can be written as

$$\frac{\partial \rho \mathbf{U}}{\partial t} + \nabla \cdot (\rho \mathbf{U}\mathbf{U}) = -\nabla p + \nabla \cdot \tau + \rho \mathbf{g} \tag{24}$$

where p is the pressure, τ is the extra-stress tensor, and $\mathbf{g}$ is the gravitational acceleration vector.

Conditional volume averaging of the momentum equation gives

$$\overline{I_\varphi \frac{\partial \rho \mathbf{U}}{\partial t}} + \overline{I_\varphi \nabla \cdot (\rho \mathbf{U}\mathbf{U})} = -\overline{I_\varphi \nabla p} + \overline{I_\varphi \nabla \cdot \tau} + \overline{I_\varphi \rho \mathbf{g}} \tag{25}$$

By again making the *a priori* assumption of incompressible fluids, as is the case for the continuity equation, one obtains

$$\begin{aligned} &\frac{\partial \alpha_\varphi \overline{\rho}_\varphi \overline{\mathbf{U}}_\varphi}{\partial t} + \widehat{\rho \mathbf{U} (\mathbf{n}_{I,\varphi} \cdot \mathbf{U}_I)} \Sigma + \nabla \cdot (\alpha_\varphi \overline{\rho}_\varphi \overline{\mathbf{U}}_\varphi \overline{\mathbf{U}}_\varphi) \\ &+ \nabla \cdot \left(\alpha_\varphi \overline{\rho}_\varphi \overline{\mathbf{U}'_\varphi \mathbf{U}'_\varphi} \right) - \widehat{\rho \mathbf{U} (\mathbf{n}_{I,\varphi} \cdot \mathbf{U})} \Sigma \\ &= -\nabla (\alpha_\varphi \overline{p}_\varphi) + \widehat{\mathbf{n}_{I,\varphi} p} \Sigma + \nabla \cdot (\alpha_\varphi \overline{\tau}_\varphi) - \widehat{\mathbf{n}_{I,\varphi} \cdot \tau} \Sigma + \alpha_\varphi \overline{\rho}_\varphi \mathbf{g} \end{aligned} \tag{26}$$

In this work, the momentum dispersion term, that is, the fourth term on the left-hand side of Eq. 26, is neglected by assuming that the flow is slow enough, which is similarly made in Sun and Beckermann.[20] Furthermore, with the assumption of no mass transfer between the phases, the two interfacial average terms on the left-hand side of Eq. 26 sum to zero resulting in

$$\begin{aligned} \frac{\partial \alpha_\varphi \overline{\rho}_\varphi \overline{\mathbf{U}}_\varphi}{\partial t} + \nabla \cdot (\alpha_\varphi \overline{\rho}_\varphi \overline{\mathbf{U}}_\varphi \overline{\mathbf{U}}_\varphi) &= -\nabla (\alpha_\varphi \overline{p}_\varphi) + \widehat{\mathbf{n}_{I,\varphi} p} \Sigma \\ &+ \nabla \cdot (\alpha_\varphi \overline{\tau}_\varphi) - \widehat{\mathbf{n}_{I,\varphi} \cdot \tau} \Sigma + \alpha_\varphi \overline{\rho}_\varphi \mathbf{g} \end{aligned} \tag{27}$$

Dividing Eq. 27 by the constant bulk density $\overline{\rho}_\varphi$, applying the product rule to the bulk pressure term according to $\nabla (\alpha_\varphi \overline{p}_\varphi) = \alpha_\varphi \nabla \overline{p}_\varphi + (\nabla \alpha_\varphi) \overline{p}_\varphi$ and grouping the interface contributed terms on the right-hand side into an interfacial momentum transfer term $\mathbf{M}_\varphi$,[27] one obtains

$$\frac{\partial \alpha_\varphi \overline{\mathbf{U}}_\varphi}{\partial t} + \nabla \cdot (\alpha_\varphi \overline{\mathbf{U}}_\varphi \overline{\mathbf{U}}_\varphi) = -\frac{\alpha_\varphi \nabla \overline{p}_\varphi}{\overline{\rho}_\varphi} + \frac{\nabla \cdot (\alpha_\varphi \overline{\tau}_\varphi)}{\overline{\rho}_\varphi} + \alpha_\varphi \mathbf{g} + \frac{\mathbf{M}_\varphi}{\overline{\rho}_\varphi} \tag{28}$$

where $\mathbf{M}_\varphi = -(\nabla \alpha_\varphi) \overline{p}_\varphi + \widehat{\mathbf{n}_{I,\varphi} p} \Sigma - \widehat{\mathbf{n}_{I,\varphi} \cdot \tau} \Sigma$. According to Eq. 18, we decompose the interfacial pressure into a mean and a fluctuation[26]

$$\widehat{\mathbf{n}_{I,\varphi} p} \Sigma = \widehat{p} \, \widehat{\mathbf{n}_{I,\varphi}} \Sigma + \widehat{\mathbf{n}^{\#}_{I,\varphi} p^{\#}} \Sigma \tag{29}$$

and by using Eq. 16 we obtain

$$\widehat{\mathbf{n}_{I,\varphi} p} \Sigma = \widehat{p} \nabla \alpha_\varphi + \widehat{\mathbf{n}^{\#}_{I,\varphi} p^{\#}} \Sigma \tag{30}$$

This results in

$$\mathbf{M}_\varphi = \left(\widehat{p} - \overline{p}_\varphi \right) \nabla \alpha_\varphi + \widehat{\mathbf{n}_{I,\varphi} p^{\#}} \Sigma - \widehat{\mathbf{n}_{I,\varphi} \cdot \tau} \Sigma \tag{31}$$

The first term can be thought of as a net force normal to the interface due to a pressure difference, whereas the last two terms can be thought of the momentum exerted due to unbalanced pressures and stresses. To obtain the correct jump conditions at the interface, the following condition must hold[20]

$$\mathbf{M}_\varphi + \mathbf{M}_\omega = \mathbf{M}_\sigma \tag{32}$$

where $\mathbf{M}_\sigma$ denotes the averaged interfacial momentum source due to surface tension, which is

$$\mathbf{M}_\sigma \equiv \sigma \widehat{\kappa_{I,\varphi} \mathbf{n}_{I,\varphi}} \Sigma \tag{33}$$

Viscoelastic two-phase flow closure

The two continuity equations (Eqs. 23) and momentum equations (Eqs. 28) (one for each phase φ and ω in a two-phase flow) together with the volume fraction equations (Eq. 17) constitute our two-phase model. Note here that only one volume fraction equation is necessary for a two-phase flow since by adding up both equations it follows that

$$\alpha_\omega = 1 - \alpha_\varphi \tag{34}$$

However, the model still includes two terms $\overline{\tau}_\varphi$ and $\mathbf{M}_\varphi$, which need proper closure models for the flow under consideration. In the following sections, we will derive closure

relations for an incompressible, isothermal, viscoelastic two-phase flow without mass transfer.

Modeling of the stress terms

We will first derive closure relations for the conditional volume averaged stress tensor $\overline{\tau}_\varphi$. We start by stating the single-phase stress equations and subsequently apply conditional volume averaging.

The fluids are assumed to obey the Oldroyd-B constitutive equation. Herein, the stress tensor for phase φ can be split into a Newtonian (solvent) contribution and a viscoelastic (polymeric) contribution as follows

$$\tau = \tau_S + \tau_P \tag{35}$$

The Newtonian law is

$$\tau_S = \eta_S\left(\nabla\mathbf{U} + (\nabla\mathbf{U})^T - \frac{2}{3}(\nabla\cdot\mathbf{U})\mathbf{I}\right) \tag{36}$$

where $\mathbf{I}$ denotes the identity matrix and η_S the solvent viscosity. Conditional volume averaging gives

$$\overline{I_\varphi\tau_S} = \overline{I_\varphi\eta_S\nabla\mathbf{U}} + \overline{I_\varphi\eta_S(\nabla\mathbf{U})^T} - \overline{I_\varphi\eta_S\frac{2}{3}(\nabla\cdot\mathbf{U})\mathbf{I}} \tag{37}$$

Applying the previously derived relationships results in

$$\begin{aligned}
\alpha_\varphi\overline{\tau_S}_\varphi &= \nabla\left(\alpha_\varphi\eta_{S,\varphi}\overline{\mathbf{U}}_\varphi\right) - \overbrace{\mathbf{n}_{I,\varphi}(\eta_S\mathbf{U})}\Sigma \\
&+ \left(\nabla\left(\alpha_\varphi\eta_{S,\varphi}\overline{\mathbf{U}}_\varphi\right)\right)^T - \overbrace{(\eta_S\mathbf{U})\mathbf{n}_{I,\varphi}}\Sigma \\
&- \nabla\cdot\left(\frac{2}{3}\alpha_\varphi\eta_{S,\varphi}\overline{\mathbf{U}}_\varphi\right)\mathbf{I} + \overbrace{\mathbf{n}_{I,\varphi}\cdot(\eta_S\mathbf{U})\mathbf{I}}\Sigma \\
&= \alpha_\varphi\eta_{S,\varphi}\nabla\overline{\mathbf{U}}_\varphi + \eta_{S,\varphi}(\nabla\alpha_\varphi)\overline{\mathbf{U}}_\varphi - \eta_{S,\varphi}(\nabla\alpha_\varphi)\mathbf{U}_I \\
&+ \alpha_\varphi\eta_{S,\varphi}\left(\nabla\overline{\mathbf{U}}_\varphi\right)^T + \eta_{S,\varphi}\overline{\mathbf{U}}_\varphi\nabla\alpha_\varphi - \eta_{S,\varphi}\mathbf{U}_I(\nabla\alpha_\varphi) \\
&- \frac{2}{3}\eta_{S,\varphi}\left\{\alpha_\varphi(\nabla\cdot\overline{\mathbf{U}}_\varphi)\mathbf{I} + \left[(\nabla\alpha_\varphi)\cdot\overline{\mathbf{U}}_\varphi\right]\mathbf{I} - (\mathbf{U}_I\cdot\nabla\alpha_\varphi)\mathbf{I}\right\}
\end{aligned} \tag{38}$$

Regrouping of the various terms leads to the closure for the Newtonian contribution $\overline{\tau_S}_\varphi$

$$\begin{aligned}
\alpha_\varphi\overline{\tau_S}_\varphi &= \alpha_\varphi\eta_{S,\varphi}\left[\nabla\overline{\mathbf{U}}_\varphi + \left(\nabla\overline{\mathbf{U}}_\varphi\right)^T - \frac{2}{3}(\nabla\cdot\overline{\mathbf{U}}_\varphi)\mathbf{I}\right] \\
&+ \eta_{S,\varphi}\left[\nabla\alpha_\varphi(\overline{\mathbf{U}}_\varphi - \mathbf{U}_I) + (\overline{\mathbf{U}}_\varphi - \mathbf{U}_I)\nabla\alpha_\varphi - \frac{2}{3}\nabla\alpha_\varphi\cdot(\overline{\mathbf{U}}_\varphi - \mathbf{U}_I)\mathbf{I}\right]
\end{aligned} \tag{39}$$

From Eq. 39, one can conclude that the average stress contains two contributions. The first term on the right represents the self-interaction of the single-phase to itself. The second term is due to the relative motion between the two phases.[20]

The polymeric contribution τ_P obeys an upper-convected Maxwell equation

$$\tau_P + \lambda\overset{\triangledown}{\tau}_P = \eta_P\left(\nabla\mathbf{U} + (\nabla\mathbf{U})^T - \frac{2}{3}(\nabla\cdot\mathbf{U})\mathbf{I}\right) \tag{40}$$

where the upper-convected time derivative $\overset{\triangledown}{\tau}_P$ is defined as

$$\overset{\triangledown}{\tau}_P \equiv \frac{\partial\tau_P}{\partial t} + \nabla\cdot(\mathbf{U}\tau_P) - (\nabla\mathbf{U})^T\cdot\tau_P - \tau_P\cdot(\nabla\mathbf{U}) \tag{41}$$

Applying conditional volume averaging leads to

$$\begin{aligned}
&\overline{I_\varphi\tau_P} + \overline{I_\varphi\lambda\frac{\partial\tau_P}{\partial t}} + \overline{I_\varphi\lambda\nabla\cdot(\mathbf{U}\tau_P)} - \overline{I_\varphi\lambda(\nabla\mathbf{U})^T\cdot\tau_P} - \overline{I_\varphi\lambda\tau_P\cdot(\nabla\mathbf{U})} \\
&= \overline{I_\varphi\eta_P\nabla\mathbf{U}} + \overline{I_\varphi\eta_P(\nabla\mathbf{U})^T} - \overline{I_\varphi\eta_P\frac{2}{3}(\nabla\cdot\mathbf{U})\mathbf{I}}
\end{aligned} \tag{42}$$

This results in

$$\begin{aligned}
&\alpha_\varphi\overline{\tau_P}_\varphi + \lambda_\varphi\frac{\partial\alpha_\varphi\overline{\tau_P}_\varphi}{\partial t} + \lambda_\varphi\overbrace{\tau_P\left(\mathbf{n}_{I,\varphi}\cdot\mathbf{U}_I\right)}\Sigma \\
&+ \lambda_\varphi\nabla\cdot\left(\alpha_\varphi\overline{\tau_P}_\varphi\overline{\mathbf{U}}_\varphi\right) + \nabla\cdot\left(\alpha_\varphi\overline{\tau'_{P,\varphi}\mathbf{U}'_\varphi}\right) - \lambda_\varphi\overbrace{\tau_P\left(\mathbf{n}_{I,\varphi}\cdot\mathbf{U}\right)}\Sigma \\
&- \alpha_\varphi\lambda_\varphi\left(\nabla\overline{\mathbf{U}}_\varphi\right)^T\cdot\overline{\tau_P}_\varphi - \alpha_\varphi\lambda_\varphi\overline{\left(\left(\nabla\mathbf{U}_\varphi\right)^T\right)'\cdot\tau'_{P,\varphi}} \\
&- \alpha_\varphi\lambda_\varphi\overline{\tau_P}_\varphi\cdot\nabla\overline{\mathbf{U}}_\varphi - \alpha_\varphi\lambda_\varphi\overline{\tau'_{P,\varphi}\cdot\left(\nabla\mathbf{U}_\varphi\right)'} \\
&= \nabla\left(\alpha_\varphi\eta_{P,\varphi}\overline{\mathbf{U}}_\varphi\right) - \overbrace{\mathbf{n}_{I,\varphi}(\eta_P\mathbf{U})}\Sigma \\
&+ \left(\nabla\left(\alpha_\varphi\eta_{P,\varphi}\overline{\mathbf{U}}_\varphi\right)\right)^T - \overbrace{(\eta_P\mathbf{U})\mathbf{n}_{I,\varphi}}\Sigma \\
&- \nabla\cdot\left(\frac{2}{3}\alpha_\varphi\eta_{P,\varphi}\overline{\mathbf{U}}_\varphi\right)\mathbf{I} + \overbrace{\mathbf{n}_{I,\varphi}\cdot(\eta_P\mathbf{U})\mathbf{I}}\Sigma
\end{aligned} \tag{43}$$

The interface terms on the left-hand side of Eq. 43 again sum up to zero, since there is no mass transfer

$$\lambda_\varphi\overbrace{\tau_P\left[\mathbf{n}_{I,\varphi}\cdot(\mathbf{U}_I - \mathbf{U})\right]}\Sigma = 0 \tag{44}$$

The stress dispersion term and the fluctuation terms, that is, the fifth, eighth, and tenth term on the left-hand side of Eq. 43, respectively, are assumed to be negligibly small, similar to the momentum dispersion term, and thus neglected.

Finally, assembling the above results and regrouping the terms, we obtain the following form of the conditional volume averaged upper-convected Maxwell equation

$$\begin{aligned}
&\alpha_\varphi\overline{\tau_P}_\varphi + \lambda_\varphi\left[\left(\frac{\partial\alpha_\varphi\overline{\tau_P}_\varphi}{\partial t}\right) + \nabla\cdot\left(\alpha_\varphi\overline{\tau_P}_\varphi\overline{\mathbf{U}}_\varphi\right)\right. \\
&\qquad\left. - \alpha_\varphi\overline{\tau_P}_\varphi\cdot\nabla\overline{\mathbf{U}}_\varphi - \alpha_\varphi\left(\nabla\overline{\mathbf{U}}_\varphi\right)^T\cdot\overline{\tau_P}_\varphi\right] \\
&= \alpha_\varphi\eta_{P,\varphi}\left[\nabla\overline{\mathbf{U}}_\varphi + \left(\nabla\overline{\mathbf{U}}_\varphi\right)^T - \frac{2}{3}(\nabla\cdot\overline{\mathbf{U}}_\varphi)\mathbf{I}\right] \\
&+ \eta_{P,\varphi}\left[\nabla\alpha_\varphi(\overline{\mathbf{U}}_\varphi - \mathbf{U}_I) + (\overline{\mathbf{U}}_\varphi - \mathbf{U}_I)\nabla\alpha_\varphi - \frac{2}{3}\nabla\alpha_\varphi\cdot(\overline{\mathbf{U}}_\varphi - \mathbf{U}_I)\mathbf{I}\right]
\end{aligned} \tag{45}$$

Once again, we see two contributions to the rate of change to the polymeric stress, a term representing the self-interaction of the phase φ with itself and a contribution from the relative motion of the two phases φ and ω.

Modelling of the averaged velocity on the φ-side of the interface $\mathbf{U}_I$ will be discussed in the next section.

Modeling of the interface morphology

The local interface unit normal vector $\mathbf{n}_{I,\varphi}$ and curvature $\kappa_{I,\varphi}$ are defined via the phase indicator function as follows

$$\mathbf{n}_{I,\varphi} = \frac{\nabla I_\varphi}{|\nabla I_\varphi|} \tag{46}$$

$$\kappa_{I,\varphi} = -\nabla \cdot \mathbf{n}_{I,\varphi} \tag{47}$$

To obtain closure for the interfacial averaged unit normal vector $\widehat{\mathbf{n}_{I,\varphi}}$ and curvature $\widehat{\kappa_{I,\varphi}}$, one could simply use volume averaging of the above equations

$$\widehat{\mathbf{n}_{I,\varphi}} = \frac{\overline{\mathbf{n}_{I,\varphi}\nabla I_\varphi}}{\overline{|\nabla I_\varphi|}} \tag{48}$$

$$\widehat{\kappa_{I,\varphi}} = \frac{\overline{\kappa_{I,\varphi}\nabla I_\varphi}}{\overline{|\nabla I_\varphi|}} \tag{49}$$

However, this would require knowledge of the exact local interfacial morphology, which is subsequently lost after using volume averaging.

To obtain an exploitable relationship, we use Eq. 16. This will be our closure for the interfacial averaged unit normal vector

$$\widehat{\mathbf{n}_{I,\varphi}} = \frac{\nabla \alpha_\varphi}{\Sigma} \tag{50}$$

By taking the absolute value of Eq. 50, we obtain

$$|\nabla \alpha_\varphi| = |\widehat{\mathbf{n}_{I,\varphi}}|\Sigma = \widehat{|\mathbf{n}_{I,\varphi}|}\Sigma \tag{51}$$

Now since $\widehat{|\mathbf{n}_{I,\varphi}|} = 1$, we obtain for the interfacial area density Σ

$$\Sigma = |\nabla \alpha_\varphi| \tag{52}$$

and by using Eq. 52 together with Eq. 50, we obtain the following closure

$$\widehat{\mathbf{n}_{I,\varphi}} = \frac{\nabla \alpha_\varphi}{|\nabla \alpha_\varphi|} \tag{53}$$

and similar

$$\widehat{\kappa_{I,\varphi}} = -\nabla \cdot \left(\frac{\nabla \alpha_\varphi}{|\nabla \alpha_\varphi|}\right) \tag{54}$$

In a study on flame wrinkling Donbar et al.[28] suggest using an inverse relationship between the interfacial area density Σ and the thickness of the flame brush. We will adopt this concept for our two-phase scenario to suppose that the thickness of the interfacial region is inversely proportional to the interfacial area density

$$\delta_I \approx \frac{1}{\Sigma} = \frac{1}{|\nabla \alpha_\varphi|} \tag{55}$$

To obtain a closure relation for the local interface velocity $\mathbf{U}_I$, we decompose the velocity into a mean and fluctuation

$$\mathbf{U}_I = \widehat{\mathbf{U}} + \mathbf{U}^{\#} \tag{56}$$

Sun and Beckermann[20] proposed a viscosity weighted linear function of the average total velocities of both phases in the case of different viscosities

$$\widehat{\mathbf{U}} = \frac{\alpha_\omega \eta_{\text{eff},\varphi}\overline{\mathbf{U}}_\varphi + \alpha_\varphi \eta_{\text{eff},\omega}\overline{\mathbf{U}}_\omega}{\alpha_\omega \eta_{\text{eff},\varphi} + \alpha_\varphi \eta_{\text{eff},\omega}} \tag{57}$$

This relation can be thought as an average no-slip condition at the interface. In the case of Newtonian fluids, one may use the simple expression $\eta_{\text{eff},\varphi} = \eta_{S,\varphi}$. However, in the case of an Oldroyd-B fluid, the effective viscosity must account for elastic effects as well. A simple, but still good approximation would be to use $\eta_{\text{eff},\varphi} = \eta_{S,\varphi} + \eta_{P,\varphi}$. This closure relation assumes the interface to behave in a viscous manner. In the course of this study, more implicit closures to explicitly account for elastic behavior of the interface were examined, such as $\eta_{\text{eff},\varphi} = \eta_{S,\varphi} + ||\overline{\tau_P}_\varphi||/||\overline{\dot{\gamma}}_\varphi||$, where $\overline{\dot{\gamma}}$ is the shear-rate tensor, or $\eta_{\text{eff},\varphi} = \eta_{S,\varphi} + ||\overline{\tau^*_P}_\varphi||/||\overline{\dot{\gamma}}_\varphi||$, where $\overline{\tau^*_P}_\varphi$ is obtained via $\frac{\overline{\tau_P}_\varphi}{\partial t} + \nabla \cdot \left(\overline{\mathbf{U}}_\varphi \overline{\tau_P}_\varphi\right) = \frac{\overline{\tau^*_P}_\varphi - \overline{\tau_P}_\varphi}{\lambda_\varphi}$. However, none of implicit methods proved to be justified and so the simpler viscous expression was chosen.

The surface fluctuation $\mathbf{U}^{\#}$ is assumed to be small and neglected in the following. Using this closure for the interface velocity, one may derive for the solvent and polymeric stress

$$\alpha_\varphi \overline{\tau_S}_\varphi = \alpha_\varphi \eta_{S,\varphi}\left[\nabla \overline{\mathbf{U}}_\varphi + \left(\nabla \overline{\mathbf{U}}_\varphi\right)^T - \frac{2}{3}\left(\nabla \cdot \overline{\mathbf{U}}_\varphi\right)\mathbf{I}\right] + \frac{\alpha_\varphi \eta_{S,\varphi}\eta_{\text{eff},\omega}}{\alpha_\omega \eta_{\text{eff},\varphi} + \alpha_\varphi \eta_{\text{eff},\omega}} \times \left[\nabla \alpha_\varphi\left(\overline{\mathbf{U}}_\varphi - \overline{\mathbf{U}}_\omega\right) + \left(\overline{\mathbf{U}}_\varphi - \overline{\mathbf{U}}_\omega\right)\nabla \alpha_\varphi - \frac{2}{3}\nabla \alpha_\varphi \cdot \left(\overline{\mathbf{U}}_\varphi - \overline{\mathbf{U}}_\omega\right)\mathbf{I}\right] \tag{58}$$

$$\begin{aligned}\alpha_\varphi \overline{\tau_P}_\varphi + \lambda_\varphi &\left[\left(\frac{\partial \alpha_\varphi \overline{\tau_P}_\varphi}{\partial t}\right) + \nabla \cdot \left(\alpha_\varphi \overline{\tau_P}_\varphi \overline{\mathbf{U}}_\varphi\right) - \alpha_\varphi\left(\nabla \overline{\mathbf{U}}_\varphi\right)^T \cdot \overline{\tau_P}_\varphi - \alpha_\varphi \overline{\tau_P}_\varphi \cdot \nabla \overline{\mathbf{U}}_\varphi\right] \\ &= \alpha_\varphi \eta_{P,\varphi}\left[\nabla \overline{\mathbf{U}}_\varphi + \left(\nabla \overline{\mathbf{U}}_\varphi\right)^T - \frac{2}{3}\left(\nabla \cdot \overline{\mathbf{U}}_\varphi\right)\mathbf{I}\right] + \frac{\alpha_\varphi \eta_{P,\varphi}\eta_{\text{eff},\omega}}{\alpha_\omega \eta_{\text{eff},\varphi} + \alpha_\varphi \eta_{\text{eff},\omega}} \\ &\times \left[\nabla \alpha_\varphi\left(\overline{\mathbf{U}}_\varphi - \overline{\mathbf{U}}_\omega\right) + \left(\overline{\mathbf{U}}_\varphi - \overline{\mathbf{U}}_\omega\right)\nabla \alpha_\varphi - \frac{2}{3}\nabla \alpha_\varphi \cdot \left(\overline{\mathbf{U}}_\varphi - \overline{\mathbf{U}}_\omega\right)\mathbf{I}\right]\end{aligned} \tag{59}$$

Modeling of the interfacial force density and momentum source

An important closure relation for the modeling of conditional volume averaged two-phase flows is the interfacial force density. In the course of the derivation, we will split the term into three parts, one stemming from surface tension, one from phase-slip, and one from drag.

First consider a two-phase scenario without flow in the case of surface tension. Using Eq. 33, we split the interface term into a surface average and fluctuation as follows

$$\mathbf{M}_\sigma = \sigma \widehat{\kappa_I \mathbf{n}_I}\Sigma = \sigma\left(\widehat{\kappa_I}\,\widehat{\mathbf{n}_I} + \widehat{\kappa_I^{\#}\mathbf{n}^{\#}}\right)\Sigma \tag{60}$$

The fluctuation term is assumed to be small compared to the interface average, that is, $\widehat{\kappa_I^{\#}\mathbf{n}^{\#}} \ll \widehat{\kappa_I}\,\widehat{\mathbf{n}_I}$. By using Eqs. 53 and 54

$$\mathbf{M}_\sigma \approx -\sigma\left(\nabla \cdot \frac{\nabla \alpha_\varphi}{|\nabla \alpha_\varphi|}\right)\nabla \alpha_\varphi \tag{61}$$

This will be our final closure for surface tension. Note that this term is in accordance to the continuum surface force model.[29]

Next, consider a flow parallel to a planar interface without gravity. In Eq. 31, the first term accounts for the pressure difference $(\widehat{p} - \overline{p}_\varphi)$ between bulk and interface. Initially, we followed Bestion,[30] who suggested a relationship

between the mean pressure difference and the square of the slip velocity according to

$$\widehat{p} - \overline{p}_\varphi = \frac{\alpha_\varphi \alpha_\omega \overline{\rho}_\varphi \overline{\rho}_\omega}{\alpha_\varphi \overline{\rho}_\omega + \alpha_\omega \overline{\rho}_\varphi} |\overline{\mathbf{U}}_\varphi - \overline{\mathbf{U}}_\omega|^2 \tag{62}$$

However, we found in this study, that this term $(\widehat{p} - \overline{p}_\varphi) \approx 0$ for any flow under consideration, which is why it is subsequently neglected.

For the second part of Eq. 31, we have $\widehat{\mathbf{n}_{I,\varphi}^{\#} p^{\#}} \Sigma - \widehat{\mathbf{n}_{I,\varphi} \cdot \tau} \Sigma$, which comprises the interfacial forces due to unbalanced pressures and stresses. We follow Sun and Beckermann,[20] who use the following expression

$$\mathbf{M}_\varphi^d = -h \frac{\alpha_\omega \eta_{\text{eff},\varphi} \Sigma}{\delta_I} \left(\overline{\mathbf{U}}_\varphi - \mathbf{U}_I\right) \tag{63}$$

That is, the interfacial Reynolds number is assumed to be small so that the drag force between the two phases is linearly proportional to the slip velocity. With the use of Eqs. 52, 55, and 57 we obtain

$$\mathbf{M}_\varphi^d = -h \frac{\alpha_\varphi \alpha_\omega \eta_{\text{eff},\varphi} \eta_{\text{eff},\omega} \left(|\nabla \alpha_\varphi|\right)^2}{\alpha_\omega \eta_{\text{eff},\varphi} + \alpha_\varphi \eta_{\text{eff},\omega}} \left(\overline{\mathbf{U}}_\varphi - \overline{\mathbf{U}}_\omega\right) \tag{64}$$

Beckermann et al.[19] proposed that $h \approx 2.5 - 2.757$, being derived for an asymptotic analysis for plane shear flow past a diffuse interface for a solid–liquid flow. The particular value depends on the profile of variation of α_φ. The same value was used for the two-phase scenario.[20] A variational analysis over two orders of magnitude showed that this value indeed results in the correct velocity profile even for two-phase flow. However, in this work, we use a value of $h = 11.028 (= 4 * 2.757)$, since after using the closure relation for $\mathbf{U}_I$ in Eq. 63 the term is proportional to $\alpha_\varphi \alpha_\omega$ having its maximum of $\alpha_\varphi \alpha_\omega = 0.25$ (at $\alpha_\varphi = \alpha_\omega = 0.5$), which is why we use a factor of four. Note that this value results also in the correct velocity profile, as will be shown in the results, however, having beneficial stabilizing features to the solution, as the coupling between the both phases in strengthened.

Using both Eqs. 61 and 64 results in the final closure of $\mathbf{M}_\varphi$

$$\mathbf{M}_\varphi = -h \frac{\alpha_\varphi \alpha_\omega \eta_{\text{eff},\varphi} \eta_{\text{eff},\omega} \left(|\nabla \alpha_\varphi|\right)^2}{\alpha_\omega \eta_{\text{eff},\varphi} + \alpha_\varphi \eta_{\text{eff},\omega}} \left(\overline{\mathbf{U}}_\varphi - \overline{\mathbf{U}}_\omega\right) - \sigma \left(\nabla \cdot \frac{\nabla \alpha_\varphi}{|\nabla \alpha_\varphi|}\right) \nabla \alpha_\varphi \tag{65}$$

Numerical Implementation

Our system of equations is described by the volume fraction equations (Eqs. 17), the continuity equations (Eqs. 23), and the momentum equations (Eqs. 28), the underlying closure relations for stress (Eqs. 58 and 59) and the interfacial momentum transfer (Eq. 65) for both φ and ω. In this section, we describe the numerical procedure to solve these equations.

Pressure reformulation

A critical issue in solving the above system of equations is the need for two pressures being strongly coupled at the interface. This would require a thorough coupled solution procedure. Now, in incompressible single-phase flows, pressure is mainly used to satisfy continuity. If a similar technique is used for a two-phase flow, then pressure will be used to guarantee overall continuity, whereas the phase fractions are obtained by the continuity equations. Therefore, we will make use of a single/mixture pressure according to

$$\overline{p} = \overline{p}_\varphi = \overline{p}_\omega \tag{66}$$

Since we then remove one unknown, we consequently have to remove an equation to stay well-posed, which will be the first volume fraction equation (Eq. 17). The second equation will be used in its transformed form as given by Eq. 34.

Furthermore, in order to smooth out the pressure field, which is necessary in the numerical procedure,[31] we will make use of a modified pressure $\overline{p^d}$ by separating out the hydrostatic pressure, $-\rho \mathbf{g} \cdot \mathbf{x}$, where $\mathbf{x}$ is the position vector and $\rho = \alpha_\varphi \overline{\rho}_\varphi + \left(1 - \alpha_\varphi\right) \overline{\rho}_\omega$. The momentum equation for quiescent fluids and flat interfaces is

$$\frac{\nabla \overline{p}}{\overline{\rho}_\varphi} = \mathbf{g} \tag{67}$$

In the case of constant gravitational acceleration $\mathbf{g}$ one may write $\nabla(\rho \mathbf{g} \cdot \mathbf{x}) = \mathbf{g} \cdot \mathbf{x} \nabla \rho + \rho \mathbf{g}$. This leads to

$$\frac{\nabla \overline{p}}{\overline{\rho}_\varphi} = \frac{\nabla \overline{p^d}}{\overline{\rho}_\varphi} + \frac{1}{\overline{\rho}_\varphi} (\rho \mathbf{g} + \mathbf{g} \cdot \mathbf{x} \nabla \rho) \tag{68}$$

Substituting Eq. 68 into the momentum equation, Eq. 28, we get

$$\begin{aligned} &\frac{\partial \alpha_\varphi \overline{\mathbf{U}}_\varphi}{\partial t} + \nabla \cdot \left(\alpha_\varphi \overline{\mathbf{U}}_\varphi \overline{\mathbf{U}}_\varphi\right) \\ &= -\frac{\alpha_\varphi \nabla \overline{p^d}}{\overline{\rho}_\varphi} + \alpha_\varphi \left(1 - \frac{\rho}{\overline{\rho}_\varphi}\right) \mathbf{g} - \alpha_\varphi \frac{\mathbf{g} \cdot \mathbf{x} \nabla \rho}{\overline{\rho}_\varphi} + \frac{\nabla \cdot \left(\alpha_\varphi \overline{\tau}_\varphi\right)}{\overline{\rho}_\varphi} + \frac{\mathbf{M}_\varphi}{\overline{\rho}_\varphi} \end{aligned} \tag{69}$$

Phase fraction equation reformulation

An important aspect in two-phase flows is to keep the phase fraction α_φ strictly bounded between zero and one. In this work, we will adopt the Weller[27] scheme by reformulating the continuity equations Eqs. 23. We, therefore, define a mixture velocity $\overline{\mathbf{U}}$ as follows

$$\overline{\mathbf{U}} = \alpha_\varphi \overline{\mathbf{U}}_\varphi + \alpha_\omega \overline{\mathbf{U}}_\omega \tag{70}$$

Combining Eqs. 23 both for φ and ω together with Eq. 70 yields the incompressibility constraint for the mixture velocity

$$\nabla \cdot \overline{\mathbf{U}} = 0 \tag{71}$$

Further, a relative velocity $\overline{\mathbf{U}}_r$ is defined according to

$$\overline{\mathbf{U}}_r = \overline{\mathbf{U}}_\varphi - \overline{\mathbf{U}}_\omega \tag{72}$$

Combining Eqs. 23, 34, 70, and 72 yields the phase fraction convection equation

$$\frac{\partial \alpha_\varphi}{\partial t} + \nabla \cdot \left(\alpha_\varphi \overline{\mathbf{U}}\right) + \nabla \cdot \left(\overline{\mathbf{U}}_r \alpha_\varphi \left(1 - \alpha_\varphi\right)\right) = 0 \tag{73}$$

It follows from Eq. 71 that the first and second convection terms in Eq. 73 are both conservative and bounded between zero and one. However, to guarantee this boundedness, Eq. 73 has to be solved fully implicitly. Since the second convection term is nonlinear in α_φ one has to adopt an iterative procedure.

Phase-intensive momentum and constitutive equation

Another important aspect on solving the above set of equations is the difficulty for solving the momentum and constitutive equations in the case when the phase fractions become zero. We, therefore, derive phase intensive forms of those equations.

Considering the momentum equation (Eq. 69), the product rule is applied to the instationary and convective terms on the right-hand side according to

$$\begin{aligned}&\frac{\partial \alpha_\varphi \overline{\mathbf{U}}_\varphi}{\partial t} + \nabla \cdot \left(\alpha_\varphi \overline{\mathbf{U}}_\varphi \overline{\mathbf{U}}_\varphi\right) \\ &= \alpha_\varphi \frac{\partial \overline{\mathbf{U}}_\varphi}{\partial t} + \overline{\mathbf{U}}_\varphi \frac{\partial \alpha_\varphi}{\partial t} + \alpha_\varphi \overline{\mathbf{U}}_\varphi \cdot \nabla \overline{\mathbf{U}}_\varphi + \overline{\mathbf{U}}_\varphi \nabla \cdot \left(\alpha_\varphi \overline{\mathbf{U}}_\varphi\right)\end{aligned} \tag{74}$$

Next, subtracting $\overline{\mathbf{U}}_\varphi$-times the continuity equation (Eq. 23) and dividing by α_φ yields

$$\frac{\partial \overline{\mathbf{U}}_\varphi}{\partial t} + \overline{\mathbf{U}}_\varphi \cdot \nabla \overline{\mathbf{U}}_\varphi = -\frac{\nabla \overline{p^d}}{\overline{\rho}_\varphi} + \left(1 - \frac{\rho}{\overline{\rho}_\varphi}\right)\mathbf{g} - \frac{\mathbf{g} \cdot \mathbf{x} \nabla \rho}{\overline{\rho}_\varphi} + \frac{\nabla \cdot \left(\alpha_\varphi \overline{\tau}_\varphi\right)}{\alpha_\varphi \overline{\rho}_\varphi} + \frac{\mathbf{M}_\varphi}{\alpha_\varphi \overline{\rho}_\varphi} \tag{75}$$

Note here that this equation is in nonconservative form for both the instationary and convective term. The convective term can numerically be evaluated as

$$\overline{\mathbf{U}}_\varphi \cdot \nabla \overline{\mathbf{U}}_\varphi = \nabla \cdot \left(\overline{\mathbf{U}}_\varphi \overline{\mathbf{U}}_\varphi\right) - \overline{\mathbf{U}}_\varphi \left(\nabla \cdot \overline{\mathbf{U}}_\varphi\right) \tag{76}$$

With respect to the numerical implementation of the stress terms, they are expanded into a pure bulk and interfacial part according to

$$\frac{\nabla \cdot \left(\alpha_\varphi \overline{\tau}_\varphi\right)}{\alpha_\varphi \overline{\rho}_\varphi} = \frac{1}{\overline{\rho}_\varphi} \nabla \cdot \overline{\tau}_\varphi + \frac{\nabla \alpha_\varphi}{\alpha_\varphi \overline{\rho}_\varphi} \cdot \overline{\tau}_\varphi \tag{77}$$

Consequently, we will need the phase-intensive form of $\overline{\tau_{S}}_\varphi$ and $\overline{\tau_P}_\varphi$.

To obtain the phase intensive solvent stress contribution, we simply divide Eq. 39 by α_φ

$$\begin{aligned}\overline{\tau_S}_\varphi &= \eta_{S,\varphi}\left[\nabla \overline{\mathbf{U}}_\varphi + \left(\nabla \overline{\mathbf{U}}_\varphi\right)^T - \frac{2}{3}\left(\nabla \cdot \overline{\mathbf{U}}_\varphi\right)\mathbf{I}\right] + \frac{\eta_{S,\varphi}\eta_{\mathrm{eff},\omega}}{\alpha_\omega \eta_{\mathrm{eff},\varphi} + \alpha_\varphi \eta_{\mathrm{eff},\omega}} \\ &\times \left[\nabla \alpha_\varphi \left(\overline{\mathbf{U}}_\varphi - \overline{\mathbf{U}}_\omega\right) + \left(\overline{\mathbf{U}}_\varphi - \overline{\mathbf{U}}_\omega\right)\nabla \alpha_\varphi - \frac{2}{3}\nabla \alpha_\varphi \cdot \left(\overline{\mathbf{U}}_\varphi - \overline{\mathbf{U}}_\omega\right)\mathbf{I}\right]\end{aligned} \tag{78}$$

Furthermore, the solvent stress is split into a diffusive and correction term in view of the numerical implementation

$$\overline{\tau_S}_\varphi = \overline{\tau_S}_\varphi|_{\mathrm{diff.}} + \overline{\tau_S}_\varphi|_{\mathrm{corr.}} \tag{79}$$

where

$$\overline{\tau_S}_\varphi|_{\mathrm{diff.}} = \eta_{S,\varphi} \nabla \overline{\mathbf{U}}_\varphi \tag{80}$$

and

$$\begin{aligned}\overline{\tau_S}_\varphi|_{\mathrm{corr.}} &= \eta_{S,\varphi}\left[\left(\nabla \overline{\mathbf{U}}_\varphi\right)^T - \frac{2}{3}\left(\nabla \cdot \overline{\mathbf{U}}_\varphi\right)\mathbf{I}\right] + \frac{\eta_{S,\varphi}\eta_{\mathrm{eff},\omega}}{\alpha_\omega \eta_{\mathrm{eff},\varphi} + \alpha_\varphi \eta_{\mathrm{eff},\omega}} \\ &\left[\nabla \alpha_\varphi \left(\overline{\mathbf{U}}_\varphi - \overline{\mathbf{U}}_\omega\right) + \left(\overline{\mathbf{U}}_\varphi - \overline{\mathbf{U}}_\omega\right)\nabla \alpha_\varphi - \frac{2}{3}\nabla \alpha_\varphi \cdot \left(\overline{\mathbf{U}}_\varphi - \overline{\mathbf{U}}_\omega\right)\mathbf{I}\right]\end{aligned} \tag{81}$$

The same approach that was applied to the momentum equation is now used for the Oldroyd-B equation. We start by applying the product rule to the instationary and convective terms of Eq. 59 to obtain

$$\begin{aligned}&\frac{\partial \alpha_\varphi \overline{\tau_P}_\varphi}{\partial t} + \nabla \cdot \left(\alpha_\varphi \overline{\tau_P}_\varphi \overline{\mathbf{U}}_\varphi\right) \\ &= \alpha_\varphi \frac{\partial \overline{\tau_P}_\varphi}{\partial t} + \overline{\tau_P}_\varphi \frac{\partial \alpha_\varphi}{\partial t} + \alpha_\varphi \overline{\mathbf{U}}_\varphi \cdot \nabla \overline{\tau_P}_\varphi + \overline{\tau_P}_\varphi \nabla \cdot \left(\alpha_\varphi \overline{\mathbf{U}}_\varphi\right)\end{aligned} \tag{82}$$

Next, substracting $\lambda_\varphi \overline{\tau_P}_\varphi$ multiplied with Eq. 23 and dividing by α_φ from Eq. 59 leads to the phase-intensive conditionally volume averaged Oldroyd-B equation

$$\begin{aligned}&\overline{\tau_P}_\varphi + \lambda_\varphi\left[\left(\frac{\partial \overline{\tau_P}_\varphi}{\partial t}\right) + \overline{\mathbf{U}}_\varphi \cdot \nabla \overline{\tau_P}_\varphi - \left(\nabla \overline{\mathbf{U}}_\varphi\right)^T \cdot \overline{\tau_P}_\varphi - \overline{\tau_P}_\varphi \cdot \nabla \overline{\mathbf{U}}_\varphi\right] \\ &= \eta_{P,\varphi}\left[\nabla \overline{\mathbf{U}}_\varphi + \left(\nabla \overline{\mathbf{U}}_\varphi\right)^T - \frac{2}{3}\left(\nabla \cdot \overline{\mathbf{U}}_\varphi\right)\mathbf{I}\right] + \frac{\eta_{P,\varphi}\eta_{\mathrm{eff},\omega}}{\alpha_\omega \eta_{\mathrm{eff},\varphi} + \alpha_\varphi \eta_{\mathrm{eff},\omega}} \\ &\times \left[\nabla \alpha_\varphi \left(\overline{\mathbf{U}}_\varphi - \overline{\mathbf{U}}_\omega\right) + \left(\overline{\mathbf{U}}_\varphi - \overline{\mathbf{U}}_\omega\right)\nabla \alpha_\varphi - \frac{2}{3}\nabla \alpha_\varphi \cdot \left(\overline{\mathbf{U}}_\varphi - \overline{\mathbf{U}}_\omega\right)\mathbf{I}\right]\end{aligned} \tag{83}$$

where the nonconservative-convection term is treated numerically as

$$\overline{\mathbf{U}}_\varphi \cdot \nabla \overline{\tau_P}_\varphi = \nabla \cdot \left(\overline{\tau_P}_\varphi \overline{\mathbf{U}}_\varphi\right) - \left(\nabla \cdot \overline{\mathbf{U}}_\varphi\right)\overline{\tau_P}_\varphi \tag{84}$$

Stabilization using the both sides diffusion

To stabilize the solution procedure due to the treatment of viscoelasticity, we use the both sides diffusion technique, which introduces an elliptic operator into the momentum equation (Eq. 75 coupled with Eq. 77), see, for example[32]

$$\begin{aligned}&\frac{\partial \overline{\mathbf{U}}_\varphi}{\partial t} + \overline{\mathbf{U}}_\varphi \cdot \nabla \overline{\mathbf{U}}_\varphi - \nabla \cdot \left(\frac{\eta_{P,\varphi}}{\overline{\rho}_\varphi} \nabla \overline{\mathbf{U}}_\varphi\right) \\ &= -\frac{\nabla \overline{p^d}}{\overline{\rho}_\varphi} + \left(1 - \frac{\rho}{\overline{\rho}_\varphi}\right)\mathbf{g} - \frac{\mathbf{g} \cdot \mathbf{x} \nabla \rho}{\overline{\rho}_\varphi} \\ &+ \frac{1}{\overline{\rho}_\varphi} \nabla \cdot \overline{\tau}_\varphi + \frac{\nabla \alpha_\varphi}{\alpha_\varphi \overline{\rho}_\varphi} \cdot \overline{\tau}_\varphi - \nabla \cdot \left(\frac{\eta_{P,\varphi}}{\overline{\rho}_\varphi} \nabla \overline{\mathbf{U}}_\varphi\right) + \frac{\mathbf{M}_\varphi}{\alpha_\varphi \overline{\rho}_\varphi}\end{aligned} \tag{85}$$

Summary of the model

Finally, assembling all the above equations yields our final set of equations describing viscoelastic two-phase flows for both φ and ω: the phase fraction convection (Eqs. 73 and 34), continuity (Eq. 71), momentum (Eq. 85 in combination with Eqs. 65, 80, and 81), and the Oldroyd-B equation (Eq. 83).

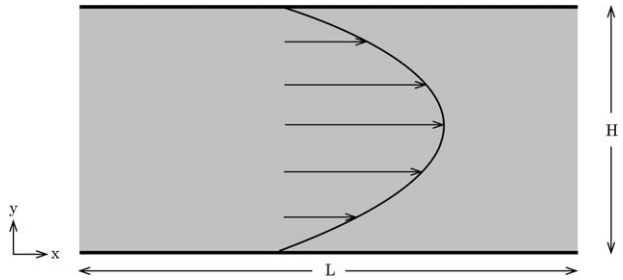

Figure 1. Domain and boundary conditions for a single-phase Poiseuille flow.

Numerical discretization

In this section, we will briefly outline the discretization practices adopted to solve the above set of equations.

The package OpenFOAM®, which is based on the finite volume method, is used. This package is capable of handling both regular orthogonal cells and nonorthogonal cells. A collocated grid arrangement is used storing all variables at the cell centers.

For temporal discretization, we use a three-point scheme giving at least second-order accuracy in time.[33]

The convective terms are discretized using the Gamma scheme with a blending factor of 0.8.[34] A study on viscoelastic single-phase flows using this scheme can be found in Favero et al.[35]

Iterative procedure

To solve the above strongly coupled set of equations, we use a pressure-implicit with splitting of operators (PISO) algorithm.[36] The iterative procedure can be summarized as follows:

1. Solve the phase fraction equation Eq. 73 for a given number of times ($n_\alpha = 2$).
2. PISO-Loop
   a. Predict the cell fluxes.
   b. Construct and solve a Poisson-type equation for pressure using Eq. 71.
   c. Correct the fluxes and velocities.
   d. Repeat from (a) for a given number of times ($n_{\text{PISO}} = 2$).
3. Solve the Oldroyd-B equations Eqs. 83.
4. If necessary, repeat from (1) until a given accuracy is met (in this work $n_{\text{total}} = 1$ is used throughout).

For pressure correction, a Preconditional Conjugate Gradient (PCG) solver with Diagonal Incomplete Cholesky (DIC) preconditioning is used at a tolerance of 10^{-12}. For the phase fraction and polymeric stress equations, a BiCGStab is used with a Cholesky preconditioner at a tolerance of 10^{-10} for phase fraction and 10^{-6} for stress, respectively.

Results and Discussion

Single phase flow

In the case of only one fluid being present, a model for multiphase-flows must behave as a single-phase model. This is, we have $\alpha_\varphi = 1$ throughout the domain. The phase fraction equation (Eq. 73) reduces to $\alpha_\varphi = \text{const}.$, whereas the second modified continuity equation (Eq. 71) reduces to the single phase incompressibility constraint $\nabla \cdot \overline{\mathbf{U}}_\varphi = 0$. No coupling interfacial terms are present, and the momentum equation for phase φ (Eq. 85) reduces to the single-phase momentum equation. The same applies to the stress models (Eqs. 81 and 83), in which the interfacial terms disappear. In this section, we will prove this behavior numerically.

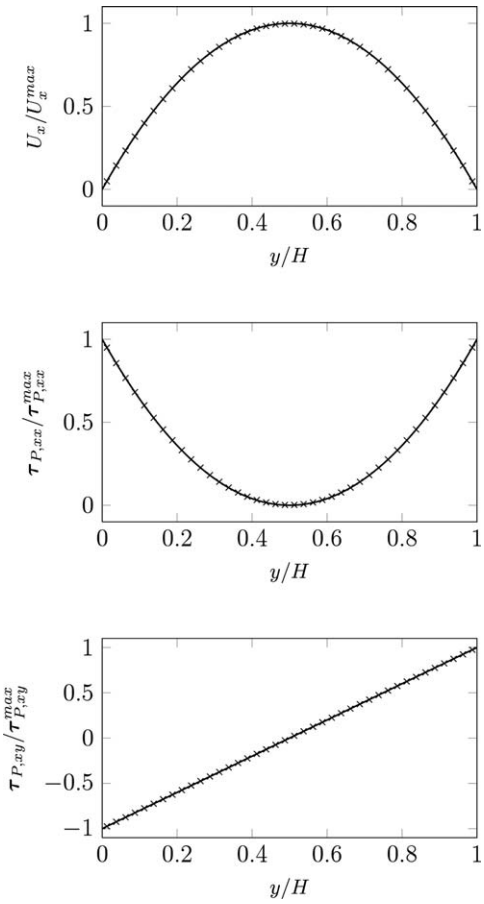

Figure 2. Single-phase flow between two parallel plates.

Solid line is the analytical solution, crosses are numerical predictions.

Therefore, consider a single-phase flow between two parallel plates due to a pressure gradient (Poiseuille-flow), see Figure 1. The retardation ratio is set to $\beta = \eta_S/\eta_0 = 0.5$ and the local Weissenberg number at the wall is chosen to be $Wi_{\text{wall}} = \lambda\dot{\gamma}_{\text{wall}} = 1$. The domain is discretized with regular hexahedra with $\Delta x/\Delta y = 1$ with 40 cells in y-direction and 20 cells in x-direction.

The results for the normalized velocity, polymeric normal, and shear stress are shown in Figure 2. The excellent agreement with the single-phase analytical solution proves that the above condition is satisfied and the single-phase model is recovered. Defining a maximum error for the quantity Φ according to

$$e_{L_\infty}^{\Phi} := \max_j^N \left(|\Phi_{\text{ana},j} - \Phi_{\text{num},j}|\right) \tag{86}$$

for N values, which correspond to the cell centered values, we obtain the error for velocity of $e_\infty^{u_x} = 1.25 \times 10^{-3}$, for the polymeric normal stress of $e_\infty^{\tau_{P,xx}} = 5.23 \times 10^{-5}$ and for the polymeric shear stress of $e_\infty^{\tau_{P,xy}} = 1.14 \times 10^{-5}$.

Shear-flow parallel to a planar interface

In this section, a two-phase shear flow parallel to a planar interface is considered to examine the coupling between the two phases and the choice of $h = 11.028$. Furthermore, the behavior of the model with mesh refinement and varying diffuse interface width is examined.

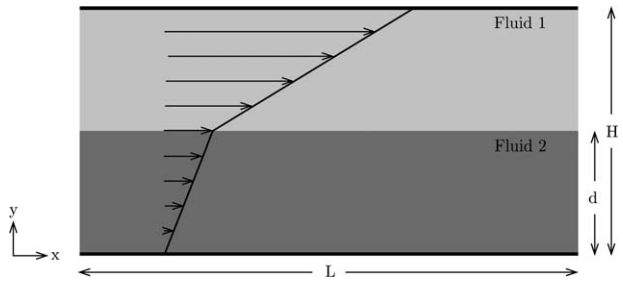

Figure 3. Domain and boundary conditions for a shear-flow parallel to a flat interface at different viscosities.

In Figure 3, the domain is shown. The fluids have a viscosity ratio of $\eta_r = \eta_2/\eta_1 = 10$. We set the retardation ratio to $\beta = 0.5$ and choose a very small relaxation time, that is, $\lambda_1 = \lambda_2 \to 0$. The upper wall moves in positive x-direction and the lower wall remains stationary, such that the interface moves in x-direction with a velocity of $(U_{I,x}/U_{\text{wall},x} = (\eta_r + 1)^{-1})$. The domain is discretized with regular hexahedra with $\Delta x/\Delta y = 1$. The diffuse interface is assigned with a tangent hyperbolic profile according to

$$\alpha_\varphi = 0.5\left(1 - \tanh\left(\frac{y - 0.5}{2\delta}\right)\right)$$

where y is the height and δ is the diffuse interface width, such that α_φ varies between 0.05 and 0.95 over 6δ .[20] The ratio of $\delta/\Delta x$ is the interfacial resolution and is proportional to the number of interface containing cells in the interface-normal direction.

The results are shown in Figure 4. In the first column, we vary the interface resolution between $\delta/\Delta x = 0.25\ldots4$ (corresponding to $H/\delta = 640\ldots40$) at a constant cell count number of $H/\Delta x = 160$ distributed over the height. We find that the velocities match the analytical profile almost perfectly, except for the case of the smallest interface width considered. In this case, the interface width compared to cell size is $\delta/\Delta x = 0.25$ corresponding to approximately two interface containing cells in the interface-normal direction. It is our understanding that in this case the coupling between the two-phases is too small resulting in an unphysical velocity profile. Provided that the interface resolution is sufficient, which in this case is $\delta/\Delta x \geq 0.5$, the velocity profiles match the analytical profile regardless of the interface width. In the middle column of Figure 4, we keep the interface resolution constant at $\delta/\Delta x = 1$ (corresponding to approximately nine interface containing cells in the interface-normal direction), which was found to be a sufficient resolution, and vary the cell number from $H/\Delta x = 10\ldots160$ in the y-direction. Here, we find that the velocities vary smoothly inside of the diffuse interface, whereas outside of the diffuse interface they are found to exactly match the analytical velocity profile. This is in accordance with the results of Ref. 20. It has to be pointed out that for the smallest cell size, the interface is distributed over the entire height of the domain, while still having nearly the correct slope at the walls. In the results shown in the third column of Figure 4, we have a constant interface width compared to the height of the domain of $H/\delta = 40$ corresponding to an interface height of approximately 0.2. Herein, we vary the cell count number in y-direction from 10 to 160, which corresponds to interfacial resolutions of $\delta/\Delta x = 0.25\ldots4$. For

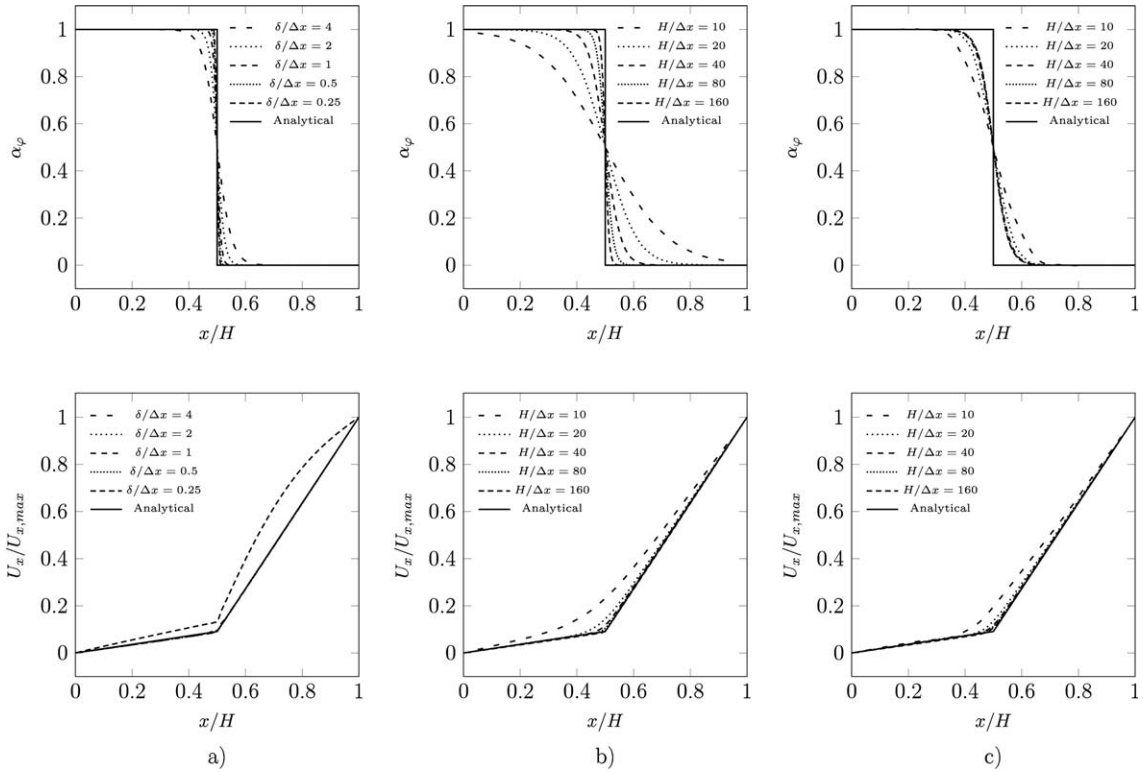

Figure 4. Volume fraction and velocity profiles across a planar interface with a shear-flow parallel to the interface at $\eta_r = 10$.

(a) $H/\Delta x = 160$ as a function of $\delta/\Delta x$, (b) $\delta/\Delta x = 1$ as a function of $H/\Delta x$, and (c) $H/\delta = 40$ as a function of $H/\Delta x (\delta/\Delta x = 1/40 \cdot H/\Delta x)$.

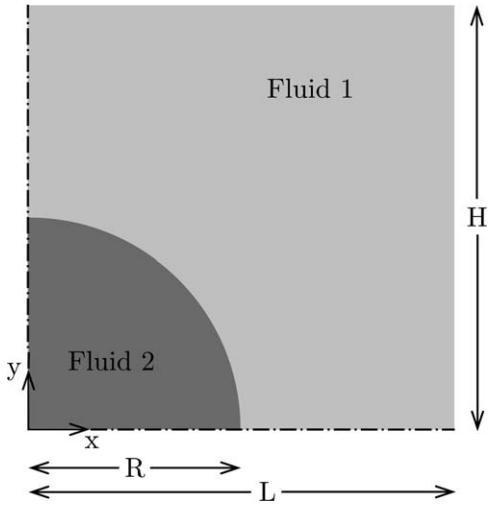

Figure 5. Domain and boundary conditions for a pressure difference due to a cylindrical interface with surface tension.

$\delta/\Delta x = 0.25$, the profile deviates from the analytical solution. However, for finer interface resolutions, we again find that the velocities match the analytical solution very well, while smoothly varying inside of the diffuse interface.

Overall, we find that a value of $h = 11.028$ is a reasonable choice, since the above results show that the analytical profile is reproduced almost perfectly. Furthermore, as a result of the above-examined behavior of the model, one may in fact choose an arbitrary interface width, which, if being sufficiently resolved, does not bias the velocity outside of it. Considering a flow of interest, the upper limit of the interface width is solely determined by the length scales of interest, that is, the characteristic curvature of the interface. This is a remarkable advantage compared to common diffuse interface methods.

Pressure jump across a cylindrical interface due to surface tension

In this section, the behavior of the surface tension closure is examined by considering a case without flow having a two-dimensional cylindrical interface with surface tension.

Consider a quadrant of length and height $L = H$, in which a cylindrical interface of $D = 2R = L$ is imposed with its center on the left bottom, as shown in Figure 5. Symmetry boundary conditions are imposed at the bottom and left-hand side.

The far-field pressure is set to $p_\infty = 0\mathrm{kg/ms}^2$ Again, regular hexahedra, that is, $\Delta x/\Delta y = 1$, are used for discretization. The diffuse interface is set up using a tangent hyperbolic profile similar to the last case.

At first, we set a constant discretization of $D/\Delta x(= L/\Delta x = H/\Delta x) = 160$ and vary the interface width such as to obtain resolutions of $\delta/\Delta x = 0.25\ldots4$, which is shown in the left column of Figure 6. Here we find that for the coarsest interface resolution, that is, $\delta/\Delta x = 0.25$, the pressure profile possesses overshoots and undershoots resulting in a profile with two kinks. Furthermore, the Young–Laplace equation is not satisfied, as can be seen from the total pressure difference. This effect attenuates with finer interface resolution, that is, $\delta/\Delta x = 0.5$, and totally disappears when $\delta/\Delta x = 1$. Furthermore, we find that for $\delta/\Delta x \geq 1$ the Young–Laplace relation is sufficiently reproduced. In the middle column of Figure 6, the interface resolution is kept at a constant $\delta/\Delta x = 1$, which, as can seen in the left column, is a sufficient resolution. We vary the cell count number in y-direction from $D/\Delta x = 10$ to $H/\Delta x = 160$. For the coarsest resolution $D/\Delta x = 10$, the interface is distributed over the total radius of the cylindrical interface resulting in a smoothed pressure profile over the whole cylinder. Furthermore, the Young–Laplace relation is not satisfied. By doubling the resolution to $D/\Delta x = 20$, the pressure profile

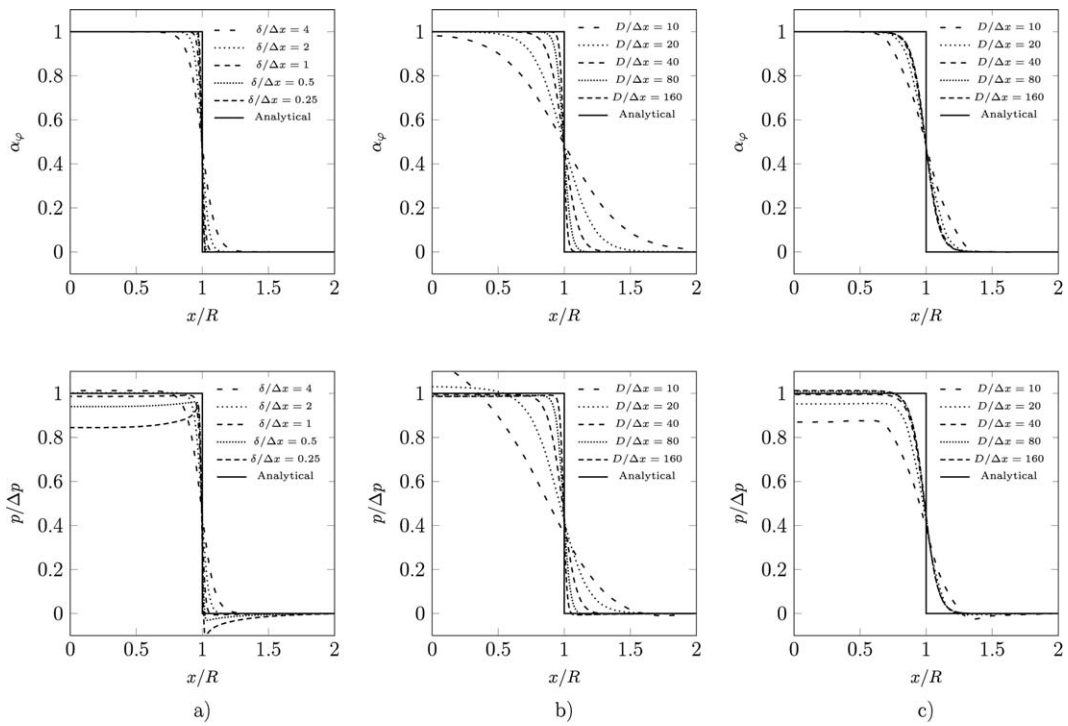

Figure 6. Volume fraction and pressure profiles across a cylindrical interface with surface tension.

(a) $D/\Delta x$=160 as a function of $\delta/\Delta x$, (b) $\delta/\Delta x$=1 as a function of $D/\Delta x$, and (c) D/δ=40 as a function of $D/\Delta x(\delta/\Delta x = 1/40 \cdot D/\Delta x)$.

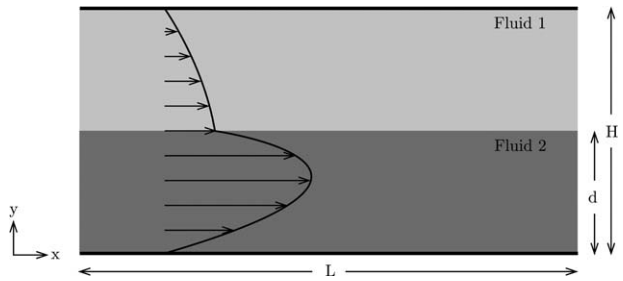

Figure 7. Domain and boundary conditions for a stratified two-phase Poiseuille flow between two parallel plates.

almost matches the analytical pressure profile outside of the diffuse interface while smoothly varying inside of the diffuse interface. From $H/\Delta x \geq 40$, we find, that the pressure profile is almost perfectly reproduced outside of the diffuse interface. Further, the volume fraction and pressure profile sharpen with further mesh refinement due to the constant interface resolution of $\delta/\Delta x = 1$. In the third column of Figure 6, we impose a constant diffuse interface width of $D/\delta = 40$ corresponding to an interface width of approximately 0.2 (with the diameter of the cylindrical interface being 1), whereas successively refining the mesh from $D/\Delta x = 10$ to $D/\Delta x = 160$ corresponding to interface resolutions from $\delta/\Delta x = 0.25$ to $\delta/\Delta x = 4$, respectively. Again, we find, that the Young–Laplace relation is satisfactorily reproduced from $\delta/\Delta x \geq 1$.

To summarize, we find that to numerically model two-phase flows with surface tension using the closure relation in Eq. 61, one needs a sufficient resolution of the diffuse interface width, that is, $\delta/\Delta x \geq 1$ corresponding to the interface being distributed over approximately nine cells. Furthermore, using an interface resolution of $\delta/\Delta x = 1$, the characteristic radius must be at least $R/\delta = 20$ (see the results of the middle column of Figure 6). However, due to the model behavior shown in the last case, one can in fact provide a sufficiently resolved interface distributed over an arbitrary number of cells, without biasing the flow outside of the interface. These results prove the capability of the model to predict large-scale flows by numerically motivated diffusion of the interfacial region without falsifying the results, which is an exceptional behavior.

Table 1. Fluid Properties

η_r	β_1	β_2	Wi_1	Wi_2
27.03	0.5	0.5	0.2059	0.2059

Mesh convergence study: Poiseuille two-phase flow

In this section, we will examine the convergence properties of the model with respect to the spatial discretization using a stratified two-phase flow due to a pressure gradient (two-phase Poiseuille flow). Note here that this is not a convection dominated flow.

The domain and boundary conditions are shown in Figure 7 with $L = 2H$ and the interface being located at $d = H/2$. The fluid properties are tabulated in Table 1 with the Weissenberg number defined as $\mathrm{Wi} = \lambda U_{x,\max}/H$. The meshes used for mesh convergence analysis are listed in Table 2.

The analytical expressions for the velocity, normal, and shear stresses are given as follows

$$\mathbf{U}_x(y) = \begin{cases} \dfrac{1}{2\eta_1}\dfrac{\partial p}{\partial x}\left(y^2 - \dfrac{H^2 + d^2(\eta_2/\eta_1 - 1)}{H + d(\eta_2/\eta_1 - 1)}y\right), & \text{for } 0 \leq y < d \\ \dfrac{1}{2\eta_2}\dfrac{\partial p}{\partial x}\left(y^2 - \dfrac{H^2 + d^2(\eta_2/\eta_{0,1} - 1)}{H + d(\eta_2/\eta_1 - 1)}y + \dfrac{(\eta_2/\eta_1 - 1)(Hd^2 - H^2 d)}{H + d(\eta_2/\eta_1 - 1)}\right), & \text{for } d < y \leq H \end{cases}$$

$$\tau_P, xx(y) = \begin{cases} 2\eta_{P,1}\lambda_1\left[\dfrac{1}{\eta_1}\dfrac{\partial p}{\partial x}\left(y - \dfrac{1}{2}\dfrac{H^2 + d^2(\eta_2/\eta_1 - 1)}{H + d(\eta_2/\eta_1 - 1)}\right)\right]^2, & \text{for } 0 \leq y < d \\ 2\eta_{P,2}\lambda_2\left[\dfrac{1}{\eta_2}\dfrac{\partial p}{\partial x}\left(y - \dfrac{1}{2}\dfrac{H^2 + d^2(\eta_2/\eta_1 - 1)}{H + d(\eta_2/\eta_1 - 1)}\right)\right]^2, & \text{for } d < y \leq H \end{cases}$$

$$\tau_P, xy(y) = \begin{cases} \dfrac{\eta_{P,1}}{\eta_1}\dfrac{\partial p}{\partial x}\left(y - \dfrac{1}{2}\dfrac{H^2 + d^2(\eta_2/\eta_1 - 1)}{H + d(\eta_2/\eta_1 - 1)}\right), & \text{for } 0 \leq y < d \\ \dfrac{\eta_{P,2}}{\eta_2}\dfrac{\partial p}{\partial x}\left(y - \dfrac{1}{2}\dfrac{H^2 + d^2(\eta_2/\eta_1 - 1)}{H + d(\eta_2/\eta_1 - 1)}\right), & \text{for } d < y \leq H \end{cases}$$

Using these expressions, we calculate the error using the L_1- and L_2-norms of the quantity Φ according to

$$e^{\Phi}_{L_1} := \frac{1}{N}\sum_j^N |\Phi_{\mathrm{ana},j} - \Phi_{\mathrm{num},j}| \tag{87}$$

$$e^{\Phi}_{L_2} := \sqrt{\frac{1}{N}\sum_j^N \left(\Phi_{\mathrm{ana},j} - \Phi_{\mathrm{num},j}\right)^2} \tag{88}$$

as well as the L_∞-error (see Eq. 86).

The rate of convergence p is calculated using the errors of two successive meshes e_1 and e_2 (with the characteristic cell length being halved).

$$p = \log_2\left(\frac{e_1}{e_2}\right)$$

The diffuse interface is assigned with a tangent hyperbolic profile. For the convergence analysis, we use the approach of having a constant $\delta/\Delta x = 1$, when refining the mesh. Note

Table 2. Meshes Used for Mesh Convergence Analysis

Mesh	Nx	Ny	$H/\Delta x$	Number of control volumes
M1	10	10	0.1	100
M2	20	20	0.05	400
M3	40	40	0.025	1600
M4	80	80	0.0125	6400

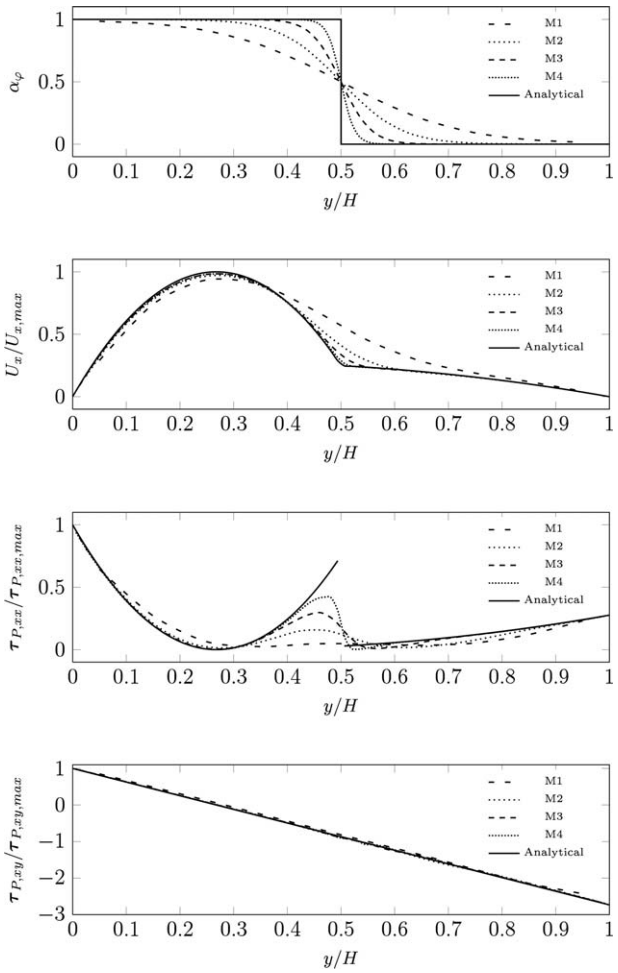

Figure 8. Volume fraction, velocity, and stress profiles of the Poiseuille two-phase flow simulation at a constant $\delta/\Delta x=1$.

that this was shown to give good results both for flows at different viscosities and flows involving surface tension, as shown in the above two cases.

The resulting volume fraction, velocity, normal, and shear stress profiles are shown in Figure 8 for the four different meshes. The diffuse interface is sharpened with mesh refinement due to the condition $\delta/\Delta x = 1$. The velocity profile is reproduced quite well, except for the coarsest mesh, in which the interface is distributed over almost the total height of the channel. With mesh refinement, we again find that the velocity smoothly varies inside of the diffuse interface, while not falsifying the solution outside of the diffuse interface. However, for the coarse mesh, we find the velocity to perceivably deviate from the analytical solution, which is due to the small spatial resolution. When considering the normal stress, we find the same behavior as we saw for the velocity, that is, the deviation reduces with mesh refinement and the profiles match the analytical solution outside of the diffuse interface, except for the coarse mesh. The jump in the normal stress is smoothed over the diffuse interface. The transition region is becoming smaller and the smoothed profile becoming steeper with mesh refinement. The necessary condition, that the jump is reproduced for $\delta \to 0$, is met. The linear shear stress profile is almost exactly predicted for all meshes.

In Table 3, the errors for velocity, normal, and shear stress are tabulated according to the above error definitions and analytical solutions. In Table 4, the rate of convergence using the errors of Table 3 are listed. No monotonic convergence can be found for the meshes under consideration, with the rates varying from approximately $p = 0.51\ldots 1.8$. Two rates are negative, indicating that the error increases with mesh refinement. For the mesh transition $M1 - M2$, the L_∞-error for the normal stress increases. Both maxima can be found in the cell next to the interface in the less viscous phase. The negativeness in p is due to the center of the cell of mesh $M2$ being closer to the interface and thus being compared to a larger value of the normal stress resulting in a larger error. The reason for the negativeness in p calculated from the L_∞-error of the shear stress for mesh transition $M3 - M4$ is that the solution tolerance for the constitutive equation is of the same order as the errors of the stress.

Conclusions

In this work, we developed a model for simulating viscoelastic two-phase flows derived from conditional volume averaging of the single-phase conservation equations. This procedure results in a set of conservation equations, one for each phase, having unclosed term. Subsequently, closure modeling is done. For the first time, we apply the aforementioned technique to a viscoelastic constitutive equation—the Oldroyd-B model— to obtain a closure for the stress. Furthermore, closures for the interfacial morphology, the momentum source due to surface tension and interfacial force density, which accounts for the viscous coupling between the

Table 3. Error Calculation for Poiseuille Two-Phase Flow Simulation

	L_1-Norm			L_2-Norm			L_∞-Norm		
Mesh	U (m/s)	τ_{xx} (N/m^2)	τ_{xy} (N/m^2)	U (m/s)	τ_{xx} (N/m^2)	τ_{xy} (N/m^2)	U (m/s)	τ_{xx} (N/m^2)	τ_{xy} (N/m^2)
1	$2.849e^{-3}$	$3.568e^{-5}$	$7.719e^{-6}$	$3.884e^{-3}$	$6.134e^{-5}$	$8.443e^{-6}$	$8.904e^{-3}$	$1.819e^{-4}$	$1.701e^{-5}$
2	$8.551e^{-4}$	$2.412e^{-5}$	$1.972e^{-6}$	$1.379e^{-3}$	$4.944e^{-5}$	$2.364e^{-6}$	$3.943e^{-3}$	$1.953e^{-4}$	$4.945e^{-6}$
3	$3.736e^{-4}$	$1.333e^{-5}$	$1.522e^{-6}$	$6.234e^{-4}$	$3.642e^{-5}$	$1.699e^{-6}$	$2.306e^{-3}$	$1.910e^{-4}$	$3.954e^{-6}$
4	$2.453e^{-4}$	$7.378e^{-6}$	$1.234e^{-6}$	$3.538e^{-4}$	$2.432e^{-5}$	$8.794e^{-7}$	$1.075e^{-3}$	$1.737e^{-4}$	$6.307e^{-6}$

Table 4. Rate of Convergence for Poiseuille Two-Phase Flow Simulation

	L_1-Norm			L_2-Norm			L_∞-Norm		
Meshes	U	τ_{xx}	τ_{xy}	U	τ_{xx}	τ_{xy}	U		τ_{xy}
M1–M2	1.736	0.565	1.969	1.494	0.311	1.836	1.175	−0.102	1.782
M2–M3	1.195	0.856	0.374	1.145	0.441	0.477	0.774	0.032	0.323
M3–M4	0.607	0.854	0.303	0.817	0.583	0.950	1.101	0.137	−0.673

two phases, are presented. This is done by splitting averaged terms into a mean part and a fluctuation part. Next, a numerical methodology was presented to solve the strongly coupled system of equations. Due to numerical issues, the equations are first reformulated.

We showed that the developed model is capable of predicting several basic test cases. Moreover, the model posseses outstanding properties. That is, the interface width may be chosen arbitrary large without falsifying the solution outside of the diffuse interface, as long as it is sufficiently resolved. This is especially necessary, if surface tension is present, for which a certain width is needed to numerically evaluate the curvature of the interface. Having that in mind, we pursued a convergence analysis for a viscoelastic two-phase Poiseuille flow by keeping the interface resolution constant while refining the mesh. Consistency and convergence were proved.

Acknowledgments

This work was supported by The Dow Chemical Company. Florian Habla gratefully acknowledges the financial support of the TUM Graduate School.

Literature Cited

1. Bryce DM. Plastic Injection Molding: Manufacturing Process Fundamentals, Dearborn, MI. *Society of Manufacturing Engineers*, 1996.
2. Utracki LA. Polymer Alloys and Blends, Munich: Hanser, 1989.
3. Rauwendaal C. Polymer Extrusion, Munich, Germany. *Hanser Fachbuch*, 2001.
4. Cristini V, Blawzdziewicz J, Loewenberg M. Drop breakup in three-dimensional viscous flows. *Phys Fluids*. 1998;10:1781–1783.
5. Anderson DM, McFadden GB, Wheeler AA. Diffuse-interface methods in fluid mechanics. *Annu Rev Fluid Mech*. 1998;30:139–165.
6. Hirt CW, Nichols BD. Volume of fluid (VOF) method for the dynamics of free boundaries. *J Comput Phys*. 1981;39:201–225.
7. Kim JM, Ahn KH, Lee SJ, Lee SJ. Numerical simulation of moving free surface problems in polymer processing using volume-of-fluid method. *Polym Eng Sci*. 2001;41:858–866.
8. Habla F, Marschall H, Hinrichsen O, Dietsche L, Jasak H, Favero JL. Numerical simulation of viscoelastic two-phase flows using OpenFOAM. *Chem Eng Sci*. 2011;66:5487–5496.
9. Sussman M, Smereka P, Osher S. A level set approach for computing solutions to incompressible two-phase flow. *J Comput Phys*. 1994;114:146–159.
10. Chang YC, Hou TY, Merriman B, Osher S. A level set formulation of Eulerian interface capturing methods for incompressible fluid flows. *J Comput Phys*. 1996;124:449–464.
11. Pillapakkam SB, Singh P. A level-set method for computing solutions to viscoelastic two-phase flow. *J Comput Phys*. 2001;174:552–578.
12. Sussman M, Puckett EG. A coupled level set and volume-of-fluid method for computing 3D and axisymmetric incompressible two-phase flows. *J Comput Phys*. 2000;162:301–337.
13. Sussman M. A second order coupled level set and volume-of-fluid method for computing growth and collapse of vapor bubbles. *J Comput Phys* 2003;187:110–136.
14. Stewart PA, Lay N, Sussman M, Ohta M. An improved sharp interface method for viscoelastic and viscous two-phase flows. *J Sci Comput*. 2008;35:43–61.
15. Unverdi SO, Tryggvason G. Computations of multi-fluid flows. *Phys D*. 1992a;60:70–83.
16. Unverdi SO, Tryggvason G. A front-tracking method for viscous, incompressible, multi-fluid flows. *J Comput Phys*. 1992b;100:25–37.
17. Yue P, Feng JJ, Liu C, Shen J. A diffuse-interface method for simulating two-phase flows of complex fluids. *J Fluid Mech*. 2004;515:293–317.
18. Yue P, Feng JJ, Liu C, Shen J. Transient drop deformation upon startup of shear in viscoelastic fluids. *Phys Fluids*. 2005;17:123101.
19. Beckermann C, Diepers HJ, Steinbach I, Karma A, Tong X. Modeling melt convection in phase-field simulations of solidification. *J Comput Phys*. 1999;154:468–496.
20. Sun Y, Beckermann C. Diffuse interface modeling of two-phase flows based on averaging: mass and momentum equations. *Phys D*. 2004;198:281–308.
21. Sun Y, Beckermann C. A two-phase diffuse-interface model for Hele-Shaw flows with large property contrasts. *Phys D*. 2008;237:3089–3098.
22. Bird RB, Armstrong RC, Hassager O. Dynamics of Polymeric Liquids, Vol. 1, 2nd ed. New York: John Wiley & Sons, 1987.
23. Dopazo C. On conditioned averages for intermittent turbulent flows. *J Fluid Mech*. 1977;81:433–438.
24. Drew DA. Mathematical modeling of two-phase flow. *Annu Rev Fluid Mech*. 1983;15:261–291.
25. Drew DA, Passman SL. Theory of Multicomponent Fluids. New York: Springer, 1999.
26. Weller HG. The development of a new flame area combustion model using conditional averaging. Technical Report; Thermo-Fluids Section Report TF 9307, Imperial College of Science, Technology and Medicine, 1993.
27. Weller HG. Derivation, modelling and solution of the conditionally averaged two-phase flow equations. Technical Report; OpenCFD Limited, 2005.
28. Donbar JM, Driscoll JF, Carter CD. Reaction zone structure in turbulent nonpremixed jet flames from CH-OH PLIF images. *Combust Flame*. 2000;122:1–19.
29. Brackbill JU, Kothe DB, Zemach C. A continuum method for modeling surface tension. *J Comput Phys*. 1992;100:335–354.
30. Bestion D. The physical closure laws in the CATHARE code. *Nucl Eng Des*. 1990;124:229–245.
31. Zhang S, Zhao X. General formulation for Rhie-Chow interpolation. In Proceeding of HT-FED04. ASME Heat Transfer/Fluids Engineering Summer Conference, Charlotte, NC, Vol. 123, 2004:131.
32. Guénette R, Fortin M. A new mixed finite element method for computing viscoelastic flows. *J Non-Newtonian Fluid Mech*. 1995;60:27–52.
33. Xue SC, Tanner RI, Phan-Thien N. Numerical modelling of transient viscoelastic flows. *J Non-Newtonian Fluid Mech*. 2004;123:33–58.
34. Jasak H. Error analysis and estimation for the finite volume method with applications to fluid flows. Ph.D. thesis; Imperial College University of London; 1996.
35. Favero JL, Secchi AR, Cardozo NSM, Jasak H. Viscoelastic flow simulation: development of a methodology of analysis using the software OpenFOAM and differential constitutive equations. *Comput Aided Chem Eng*. 2009;27:915–920.
36. Issa RI. Solution of implicitly discretised fluid flow equations by operator-splitting. *J Comput Phys* 1986;62:40–65.

Manuscript received Sep. 14, 2012, and revision received Jan. 26, 2013.